Tutor/s

Dr. Jordi Cirera
Departament de Química Inorgànica i Orgànica

Grau de Química

Treball Final de Grau

Computer assisted design of new [Cr^{II}(R-indenyl)$_2$] molecules with Spin-crossover properties

Disseny assistit per ordinador de noves molècules [Cr^{II}(R-indenyl)$_2$] amb propietats de transició de spin

Fileto Rodríguez Barba

Juny 2020

Universitat de Barcelona

B:KC Barcelona Knowledge Campus
Campus d'Excel·lència Internacional

Is therefore remarkable, that the greatest scientific revolution of all time has gone largely unnoticed by the general public, not because its implications are uninteresting, but because they are so shattering as to be almost beyond belief- even to the scientific revolutionaries themselves

Paul Davies – Other worlds

Voldria agrair al Jordi Cirera l'ajut que m'ha donat en tot moment al llarg d'aquest TFG i la seva dedicació, que han fet possible aquest treball.

REPORT

CONTENTS

1. SUMMARY

Since its discovery, spin-crossover compounds have attracted attention due to their intrinsic applications as molecular switches. These compounds have two electronic states which can be accessed with similar energies, causing that an external stimulus can determine which one becomes the predominant.

Present work explores the spin-crossover properties of indenyl chromium (II) compound, as some of them exhibit thermally induced spin-crossover transition despite having a rather than unusual metallic centre in the field of spin-crossover properties. To do so, density functional theory and ab initio ligand field theory calculations are performed, with the aim to identify the trends caused by the influence of functionalization of indenyl ligand.

The final goal of the present work is the design of new indenyl chromium (II) compounds with spin-crossover properties and tailored transition temperatures.

Keywords: Spin-crossover, chromium (II), indenyl, density functional theory, DFT, ab initio ligand field theory, AILFT, in-silico design, complexes.

2. RESUM

Des del seu descobriment, els complexes amb propietats de transició d'espín han suscitat l'interès de la comunitat científica a causa de les seves aplicacions com a interruptors moleculars. Aquests compostos posseeixen dos estats electrònics accessibles amb energies similars, fet que fa que mitjançant un estímul extern es pugui modular quin dels dos estats predomina.

El present treball explora les propietats de transició d'espín de la família de complexes d'indenil de crom (II), alguns dels quals presenten transició d'espín induïda tèrmicament amb un nucli metàl·lic poc estudiat en el camp dels materials amb propietats de transició d'espín. Per fer-lo s'empren càlculs de teoria de funcionals de densitat i teoria de camp lligand ab initio amb la intenció d'identificar les tendències derivades de la funcionalització dels lligands d'indenil.

L'objectiu final d'aquest treball es el disseny de nous sistemes capaços de presentar propietats SCO amb temperatures de transició a mesura.

Paraules clau: transició d'espín, crom (II), indenil, teoria de funcionals de densitat, DFT, teoria de camp lligand ab initio, AILFT, complexes, disseny in-silico.

3. INTRODUCTION

Coordination compounds have been known for more than two centuries, almost since modern chemistry was born. During this time, they have been widely used, due to their attractive properties, which allow a wide variety of applications. Dyes (such as Prussian blue, the first known synthetic dye, formed by a $[Fe(CN)_6]^{4-}$ salt) or homogeneous catalysts (as Ziegler-Natta catalysts, granting Karl Ziegler and Giulio Natta the 1963 Nobel prize in chemistry, which allow the homogeneous catalysis of some olefins polymerization or Suzuki's reaction catalyst, an organometallic palladium catalyst involved in Suzuki coupling reaction, with great importance in nowadays industrial chemistry which granted it's discoverers the 2010 Nobel prize in chemistry) are just some of the compound families which heavily rely on coordination complexes.

One of the more interesting properties of complexes is the way they interact with magnetic fields as, due to its own nature, d-orbitals of the metallic centre are split in subsets depending on the ligand field which they are put on. This ligand field is formed by the influence the ligands exert over the metallic centre; therefore, ligand field affects the electronic structure of the whole complex. As the electronic structure is determined by the ligand field, electrons will arrange in the split d-metal orbitals depending on how they are arranged. This fact allows the existence of compounds which exhibit diamagnetic behaviours, because all their electrons are paired, and compounds containing the same metallic centre which, due to how the ligand field they possess splits their d-orbitals, remain with some unpaired electrons, and therefore exhibit paramagnetic behaviour.

But once more, things are more complex that they seemed to be at a first glance, and some other compounds, known as SCO complexes, possess a ligand field which allows the existence of, with a certain metallic centre, two similar in energy electronic states. Therefore, these complexes can access one or another, usually influenced by an external stimulus. Depending on which one is the predominant in the specified conditions, these compounds will exhibit one or another properties, such as colour, bond lengths, angles and electromagnetic properties (the one linked to the present electronic structure).

Above exposed properties make them perfect to act as molecular switches, as their properties will change depending of an external stimulus, being the most common temperature (even if some SCO complexes have reported this behaviour under light or pressure changes).

Even though, the tunability of the temperature at which both electronic states are equally favoured (known as SCO temperature) remains to be the cornerstone for its technological application. Control over this temperature, allows the design of tailor-made compounds, exhibiting different behaviours over and under the variable.

From this perspective, and over the past decades, more and more SCO compounds have been discovered, in order to identify its trends and to get a wider and richer spectrum of temperatures and molecules[1].

4. OBJECTIVES

The principal objective of this study is the obtention of enough data to find trends in the SCO temperature of indenyl chromium (II) family of compounds, as it is a relatively new and unknown group of compounds in the field of SCO properties. These trends would be used to create new tailor-made compounds leading to a deeper knowledge about the SCO properties in chromium (II) complexes.

Regarding to specific objectives the present work aims to.

- Find a suitable methodology in order to obtain structural and SCO properties of the studied systems, in order to compare them to the bibliographically reported and validate our computational methodology.
- Identify the trends followed by indenyl chromium (II) complexes when the indenyl ligand is functionalized via the addition of methyl groups or its substitution by others.
- To analyse the orbital energy changes suffered by the studied compounds via AILFT, in order to obtain a deeper knowledge in how functionalization of ligands affects the SCO properties of certain systems.

5. THEORETICAL METHODS

5.1. AB INITIO METHODS

Ab initio methods are the ones which relies on unquestionable first principles. Many of the methods based on quantum mechanics, as the ones used in the present job, are ab initio, as they use well stablished and studied bases, which have been widely tested, and which conform the basis of most of our actual knowledge about chemistry. Questioning them, therefore, would be the same as questioning the basis of our scientific knowledge.

Quantum chemistry methods support the premise that all the information of a given system can be contained in a wavefunction, noted as Ψ. Those functions give no information directly from the system. To obtain the properties of those, one must apply a determined operator which will extract a given system property value.

One of the main properties of a system is its total energy, and hence one of the chief goals of most of quantum mechanical methods in chemistry, obtained after solving the time independent Schrödinger equation as an eigenvalue.

$$\hat{\mathrm{H}}\Psi = E\Psi \tag{1}$$

Where $\hat{\mathrm{H}}$, being the Hamiltonian operator, applied to the wavefunction, Ψ, brings the energy of the system as an eigenvalue after solving the equation.

Hamiltonian operator is described as the mathematical tool used to obtain the whole energy of a system, potential and kinetic. Those contributions to the total energy can be separated, in potential terms and kinetic terms, and furthermore, in electron and nuclei terms, leaving us the Hamiltonian decomposed in its fundamental terms as:

$$\hat{H} = \widehat{V_{nn}} + \widehat{V_{ne}} + \widehat{V_{ee}} + \widehat{K_e} + \widehat{K_n} \tag{2}$$

Where $\widehat{V_{ee}}$ and $\widehat{V_{nn}}$ refer to the potential between electrons and nuclei respectively (being that of Coulombic nature, and therefore a repulsive interaction between them as the have equal charges), $\widehat{V_{en}}$ to the Coulombic attraction potential created between nuclei and electrons due to its opposite charges. After them, there are the kinetic contributions namely, $\widehat{K_e}$ and $\widehat{K_n}$, of electrons and nuclei respectively.

Hamiltonian can be further simplified by taking advantage of the enormous mass difference between electrons and nuclei (being electrons 1836 times lighter than the lightest of nuclei in ^{1}H). In practice this means that, to a good approximation, we can consider the electrons move in a

field of fixed nuclei, reducing $\widehat{K_n}$ to 0 and $\widehat{V_{nn}}$ to a constant value as position coordinates do not change for nuclei. Schrödinger equation is therefore transformed into electronic Schrödinger equation as:

$$\widehat{\mathrm{H}_{elec}}\Psi_{elec} = E_{elec}\Psi_{elec} \quad (3)$$

Thus, obtaining the electronic energy. The total energy of the system can be calculated as the sum of E_{elec} and E_{nuc}, being E_{nuc} a merely constant value which depends of the position of each nuclei. This approximation is well known as the clamped nuclei Born Oppenheimer approximation.

We will see below how the term $\widehat{V_{ne}}$ is crucial in Density Functional Theory, often termed as external potential, V_{ext}.

5.2 Electronic density

Electronic density is defined, for a determined system, as the probability to find any electron in a volume element $d\overrightarrow{r_1}$ with arbitrary spin while the rest of the electrons in the system are in the any position and spin allowed by the wavefunction, Ψ. Differently to the wavefunction, the electronic density is an observable measure, and as all the electrons are indistinguishable the probability of finding an electron is N times the probability of finding a determined electron, where N is the total number of electrons in the system.

5.3 Density functional theory

As wavefunctions can't be resolved analytically for systems beyond the hydrogen atom, in order to find the properties of a determined system we must find alternative methods to approximate its solutions. DFT is an alternative method to describe a system, replacing Hartree-Fock and post Hartree-Fock methods which were widely used before Hohenberg and Kohn proposed the two theorems of DFT, which states that for every electronic system its energy can be calculated from its electronic density, a function which only depends from 3 spatial variables and 1 spin variable, instead that the 3N spatial variables which supports the Schrödinger equation, being N the number of electrons in the system. This makes DFT a much less power demanding method when we refer to computational calculations, allowing us to describe and calculate properties of bigger systems than the ones we could achieve with HF methods.

As said before, DFT relies on two theorems developed by Hohenberg and Kohn in 1964[2].

5.3.1 First Hohenberg Kohn theorem

The first Hohenberg and Kohn theorem specifies that the external potential felt by an electron can be expressed as a unique functional of the electronic density and backwards.

The most common way to proof it is by reductio ad absurdum, as Hohenberg and Kohn proposed it in its initial article. To probe it two external potentials, V_{ext} and V'_{ext} which differ from more than a constant, but both give rise to equal electron densities $\rho(\vec{r})$ are compared. The wavefunction of the first state ψ cannot be equal to the second one ψ' as they satisfy different Schrödinger equations. Resolving them by applying their own Hamiltonians would lead to the inconsistency $E + E' < E + E'$.

Hence no two different external potential, V_{ext}, can lead to the same ground state electronic density $\rho(\vec{r})$ and the electronic density of a system uniquely specifies the external potential.

5.3.2 Second Hohenberg Kohn theorem

Thanks to the variational principle, core in quantum mechanics, the second Hohenberg Kohn principle appears. It states that for a system only its exact electronic density will deliver the lowest energy. Otherwise, every other electronic density will deliver a higher value.

$$E_0 \leq E_{[\tilde{\rho}]} = T_{[\tilde{\rho}]} + E_{Ne[\tilde{\rho}]} + E_{ee[\tilde{\rho}]} \quad (4)$$

In other words, for a trial electronic density, $\tilde{\rho}$, the exact minimum energy, E_0, will be delivered only, and only if the if the trial electronic density is exactly the same as the exact electronic density for the system, otherwise it will be higher.

5.3.3 Kohn Sham method

One year after the proposal of the two Hohenberg Kohn theorems which became the base of density based methods and now with Lu Jeu Sham, Walter Kohn and him developed the mathematical formalism required to write down the electronic density[3].

Kohn Sham method relies on the separation of the contributions to the total energy as:

$$E[p(r)] = T_s[p(r)] + E_{ext}[p(r)] + J[p(r)] + E_{xc}[p(r)] \quad (5)$$

By doing so, one can separate the three first contribution; being $T_s[p(r)]$ the kinetic energy of the electrons in a non-interacting system, $E_{ext}[p(r)]$ the attraction felt by the electron density due to the external potential and $J[p(r)]$ the coulombic repulsion felt by electrons due to the presence of the other ones, from the $E_{xc}[p(r)]$ which refers to the correlation energy regarding to the electronic exchange and correlation effects. This last term is the only one that is unknown, being a key element in density functional methods, as it is the only one that must be truly approximative.

5.3.4 Correlation exchange functionals

The last term extracted in the above section deals with the exchange and correlation contributions to the total energy of the system. These can be separated.

$$E_{xc}[p(r)] = E_x[p(r)] + E_c[p(r)] \quad (6)$$

Where $E_x[p(r)]$ is the exchange contribution and $E_c[p(r)]$ is the correlation contribution.

These exchange correlation functionals, which has been developed since the start of DFT methods, can adopt different approaches.

The first one which was used in the early days of DFT and was LDA, the acronym of local spin density approximation. The approximation to the exchange correlation energy in LDA approach depends only from the coordinates, r.

$$E_{xc}^{LDA}[n\uparrow, n\downarrow] = \int dr\, n(r)\epsilon_{xc}^{LDA}[n_\uparrow(r), n_\downarrow(r)] \quad (7)$$

LDA methods tended to show some systematic errors which were tried to be mended by GGA approach, acronym of General gradient approximation. GGA implies that the functional used to calculate the correlation exchange energy is rewritten to add to LDA the spatial variation, the gradients, of the electronic densities.

$$E_{xc}^{GGA}[n\uparrow, n\downarrow] = \int dr\, n(r)\epsilon_{xc}^{GGA}[n_\uparrow(r), n_\downarrow(r), \nabla n_\uparrow(r), \nabla n_\downarrow(r)] \quad (8)$$

The last big framework included in the exchange correlation functionals, and the one with the higher complexity among them, is meta-GGA, which adds to GGA's energy the contribution of the so-called Kohn Sham kinetic energy density, $\tau_{\uparrow/\downarrow}(r)$[4].

$$E_{xc}^{mGGA}[n\uparrow, n\downarrow] = \int dr\, n(r)\epsilon_{xc}^{GGA}[n_\uparrow(r), n_\downarrow(r), \nabla n_\uparrow(r), \nabla n_\downarrow(r), \tau_\uparrow(r), \tau_\downarrow(r)] \quad (9)$$

There are some correlation exchange functionals which add to the energy a contribution of Hartree-Fock energy,

$$E_x^{HF} = \frac{1}{2}\sum_{i,j}\int dr \int dr' \frac{\phi_i^*(r)\phi_j^*(r')\phi_i^*(r')\phi_j^*(r)}{|r-r'|} \quad (10)$$

Into the exchange correlation energy,

$$E_{xc}^{hyb} = (1-\alpha)E_{xc}^{GGA} + \alpha E_x^{HF} \quad (11)$$

These GGA functionals perform better for some systems but are more power demanding methods.

5.4 SPIN AND QUANTUM NUMBERS

Together with the understanding of the quantum world, one crucial property was discovered. Spin can be defined, as the amount of angular momentum which is carried by a particle in a certain moment. This property can be measured for electrons, nuclei and other particles. For electrons it is defined thanks to the fourth quantum number, each one of them determining one of the properties of the electron. For an electron, as they have a total spin of $\frac{1}{2}$, the spin quantum number, written as m_s, must be either $\frac{1}{2}$ or $-\frac{1}{2}$

Electronic spin (defined as the amount of spin carried by electrons) is an important quantity in the understanding of chemical and physical behaviours of a material as especially magnetic and electric properties as they are almost entirely determined by them.

5.5 d-METAL COMPLEXES

The systems being studied in the present work belong to the huge field of knowledge of the metal complexes. Those molecules can be understood as the product of a reaction between a Lewis acid and a Lewis base, where the base (also known as ligand) creates a donative bond with the acid (being this the d metal). Regarding to the ligand, those are molecules with exposed electronic density, which is used in the creation of the bond with the acid. d-metals turn out to be perfect Lewis acids as their d-orbitals are not filled, so they can settle in the electronic density, which is being donated by the ligand, thus stabilizing the whole system.

Since their discovery, thousands of coordination compounds have been reported, possessing a wide range of applications, from medicine (as the Prussian blue, an hexacyanoferrate complex which has been classified by the WHO as an essential medicine for its antidote properties) to industrial catalysis (as Ziegler-Natta catalysts, which are used for the polymerization of alpha-

olefins in one of the most important industrial procedures known, and which discovery awarded both Carl Ziegler and Giulio Natta with the Nobel prize in chemistry at 1963).

A wide range of properties has been reported for these compounds making them especially appealing. These properties depend directly form the nature of the system, being the main variables the charge of the metallic centre, the nature of the ligands (size, hapticity and specially their electron donative power) and the coordination number.

The coordination number is defined as the number of atoms, molecules or ions bonded to it. In the field of coordination complexes, it is the number of ligands bonded to the metallic ion. Complexes with coordination number ranging from 1 to 15, being the more frequent 4, 6 and 8, have been reported.

As the d orbitals are filled with the electronic density donated by the ligands, the d orbital degeneracy is lost, separating the five metallic d orbitals into two groups, ones being nonbonding orbitals and the other ones being antibonding orbitals. How these are separated and how many are in each group depends from the coordination number and the spatial arrangement of the ligands.

5.5.1 Aromatic ligand complexes

Two more simple cases, in coordination compounds, are known to be those with octahedral and tetrahedral geometries. These geometries, force the d metal orbitals to split into two subsets, being one t_{2g} and the other one e_g. In this work we centre our attention in a similar geometry, the one achieved when two ligands donate electronic density located in an aromatic system. Compounds present in this work are homoleptic (both ligands are equal) double-deckers (they are formed by one metallic centre).

In these compounds, d metal orbitals are split into three subsets; e_{1g}, e_{2g} and a_{1g} as the two ligands are placed face to face in both sides of the metal, fact that grants them their name as sandwich compounds. These two ligands can be places even in staggered, gauche or eclipsed conformation depending on the dihedral angle between them.

The energy difference between both the nonbonding and antibonding orbitals is defined as 10Dq and is an important measure for the comprehension of the electronic structure of coordination complexes, and its physical properties to extent. As d^4 to d^7 complexes can arrange their electrons

in the molecular orbitals formed due to d metal orbitals splitting in two different ways (known as low-spin and high-spin case), having each one of them different properties, one can understand why 10Dq is an interesting magnitude. Once the three first electrons are fitted in the nonbonding orbitals, the fourth one faces a special restriction which is kept and must be considered for the next three electrons until we reach seven of them. When the new electron is placed two energetic contributions compete. The first one being our now known 10Dq and the second one being the energy arising from the repulsion felt by an electron when it forms an orbital with the same three first quantum numbers (related to the position of the particle) as another one, a coulombic contribution which is named "spin pairing energy" or P.

Therefore, if P is higher than 10Dq electrons would be preferably placed in a higher energy empty orbital rather than in the lower energy half-empty one, leading to the formation of a high-spin complex.

On the other hand, if 10Dq is higher than P, electrons will prefer to fill the half-empty orbital rather than be in the higher energy empty one, leading to the formation of a low-spin complex.

5.5.2 Magnetic properties

As has been said before, magnetic properties are almost entirely determined by the electronic structure of a material. As electrons behave as tiny magnets due to its spin and charge the ones which remain uncoupled compute for the total macroscopic magnetic susceptibility allowing us to determine whether a certain coordination compound is a low-spin compound or a high-spin compound.

The total effective magnetic susceptibility, can be calculated as:

$$\mu_{eff} = (\vec{L}(\vec{L}+1) + 4\vec{S}(\vec{S}+1))^{\frac{1}{2}}\,\mu_B \tag{12}$$

Where $\vec{L}$ represents the angular moment, and $\vec{S}$ the total spin of the system.

Where the spin-only contribution can be approached as:

$$\mu_{so} = 2(S(S+1))^{\frac{1}{2}}\,\mu_B = (n(n+2))^{\frac{1}{2}}\,\mu_B \tag{13}$$

Where S equals the total spin quantum number (calculated as the number of unpaired electrons times the spin of them, being that last $\frac{1}{2}$, this leading us to the second expression where the total spin quantum number has been substituted for the sake of simplicity, by the number of unpaired electrons).

5.5.3 Spin Cross-over Properties

As just commented when 10Dq is higher than P, electrons will stay in the lower energy orbitals even if they have to surpass the energetic barrier owing to share the three first quantum numbers with another electron (which means the two of them are sharing the spatial arrangement as said before). Therefore, the compound will expose low-spin behaviour.

Despite that, there are a whole family of compounds where the energy difference between P and 10Dq is so low, that electrons can be promoted to the higher energy orbitals due to external energetic contributions[1]. This phenomenon can be achieved via thermal energy, pressure and light[5].

In these cases, the contribution of the external effect together with the spin pairing energy P can lead to the formation of high spin complexes over required circumstances.

$$If\ E_{ext} + P < 10Dq\ \rightarrow Low\ spin$$

$$If\ E_{ext} + P > 10Dq\ \rightarrow High\ spin$$

5.5.3.1 Temperature induced spin cross-over

As said before, a small group of variables are known to have the capacity to make SCO (spin cross-over) compounds to change its spin. The principal of them, as most of the compounds known to possess this behaviour show it under variations of this variable, is temperature.

This transition, being a phase transition, can be understood as a thermochemical equilibrium determined by its Gibbs free energy[6] which can be calculated as:

$$\Delta G = G^{HS}(T) - G^{LS}(T) \quad (14)$$

Where the Gibbs free energy of each state can be obtained as:

$$G^{i}(T) = H^{i} - TS = E^{i}_{el} + E^{i}_{vib} - TS \quad (15)$$

Being E^{i}_{el} the electronic energy of the system, E^{i}_{vib} the vibrational energy and S the entropy of the whole state, leaving as only variable the temperature, T.

Gibbs free energy, will tend to be 0, approaching and reaching equilibrium at a determined temperature which can be calculated as:

$$T_{1/2} = \frac{\Delta H}{\Delta S} \quad (16)$$

$T_{1/2}$, also named T_{HALF} or SCO temperature is the temperature at which the equilibrium between the two states, low spin and high spin is reached, and therefore half of the molecules of the system is in each of the two states. Above this temperature most of the molecules of the system will adopt the high spin electronic configuration and bellow this temperature the low spin state will be the predominant in the molecules of our system.

Thanks to the variation of the properties associated with the change of the electronic structure of the molecule due to SCO properties, a wide variety of applications arise, being the most prominent the creation of molecular switches[7].

5.6 AILFT (AB INITIO LIGAND FIELD THEORY)

The present work relies on AILFT to compute the energies associated to electronic orbitals and wavefunctions at a NEVPT2 level.

Density functional theory has proven, over the past 40 years, to be a reliable and powerful tool widely used in computational modelling and tackling problems whose quantum nature hindered their resolution with another methodologies. Even though, DFT presents a problem when computing some properties, as its mono determinantal nature, do not allows it to work with wavefunctions belonging to fundamental states composed by multiple multiplicities contributions. DFT presents another problem, as their virtual orbitals (those which are not occupied) tend to overestimate their own energies, leading to unrealistic HOMO-LUMO gaps (which possess a major importance in complexes and specially in SCO properties as 10Dq is decided by this gap).

To get over it NEVPT2 and CASSCF were born, as it allows fundamental states composed by different multiplicities and thus leading to more realistic orbital energies, HOMO-LUMO and 10Dq values to an extent. That kind of calculations, even if they are powerful and necessary to resolve some problems, can lead to very complicated wavefunctions, whose interpretation requires vast knowledge about them.

AILFT acts then, as a sort of interface allowing the obtention of ligand field parameters from CASSCF and NEVPT2 ab initio calculations as well as energies associated to each orbital, in a more user friendly manner, by extracting the data in a ligand-field type matrix with the contribution and energy of orbitals resulting from the splitting of metallic d-orbitals[8].

6. COMPUTATIONAL DETAILS

All present DFT calculations have been carried using Gaussian® 09 program suite, revision D.01. Due to the absence of a clear candidate to the best exchange-correlation functional for the study of the proposed systems eight different functionals were benchmarked. Even when OPBE and TPSSh have successfully been used to model SCO processes with transition-metal complexes, the ones which are being modelled in this work have not been studied before with DFT methods, so benchmarking has been necessary. Geometry optimization calculations were performed with bis(1,2,3-trimethylindenyl) chromium (II) using each proposed functional. From the results, the difference in the energy between low-spin and high-spin state have been calculated to elucidate which one of them better performed capturing the subtle changes in the electronic structure of the compound. Def2TZVP basis set has been used for the benchmarking of each functional.

As pure exchange-correlation functionals OLYP, OPBE, BLYP, M06L and TPSSTPSS (using TPSS functionals as both exchange and correlation) were used.

Hybrid functionals were used too. In this category TPSSh, B3LYP and B3LYP* (a modification of B3LYP where Hartree-Fock was reduced changing the mixing factor from X to X).

Geometry optimizations with GD3BJ empirical dispersion were performed using the two more promising functionals, TPSSTPSS and TPSSh, in an attempt to improve their performance.

Benchmarking was made for different basis sets with TPSSTPSS functional, and, TPSSh with GD3BJ empirical dispersion correction to determine the saturation point for each of both functionals. Basis sets used were Def2TZV, Def2TZVP, Def2TZVPP, Def2QZV and Def2QZVP.

All benchmarking optimizations have been performed using a 10^{-8} convergence criterion for the density matrix elements.

For geometry optimizations and frequencies calculations correlation-exchange functional TPSSh with GD3BJ empirical dispersion correction have been used as it proved to be the most accurate of all the ones which were benchmarked.

The energy of each spin orbital was calculated using Orca electronic structure package, with AILFT methodology.

Computations of SCO temperatures have been done thanks to the Gibbs free energy difference between HS and LS states (from eq.14). For the computing of Gibbs free energy for each state the equation exposed below was used (eq. 17)

$$G^S(T, V_i) = E_{el}^S + k_B T \sum_{\upsilon_i}^{N} \ln(1 - e^{-(h\upsilon/k_B T)}) \quad (17)$$

Where E_{el}^S is the electronic energy of the system, k_B is Boltzmann's constant, T is the temperature of the system, h is Planck's constant and υ is the vibration frequency.

In order to obtain the Gibbs free energy of each system all frequencies must be considered (as they are key for the entropy contribution to the system). With more than 100 different frequencies for each individual system, and therefore more than 100 individual contributions to the summation conforming the entropy (N>100), and having to calculate the total Gibbs energy for both systems in a wide scale of temperatures the elected methodology to manipulate this huge amount of data was the creation of a Python3 script capable of reading the frequencies, performing the whole treatment of them, calculating the Gibbs free energy of the system in a specified by the user range of temperatures and express the results in a text file for the user to access them.

Firstly, a bash script was prepared in order to get the electronic energy of the system, as well as the frequencies of the system. It saved the converged electronic energy in a file called energy.txt and the frequencies in three individual .txt files named freqs1.txt, freqs2.txt and freqs3.txt containing each one third of the total frequencies.

After this data collection phase, the python3 script (presented in appendix 1) is executed.

This script starts reading the entire collection of frequencies extracted from the three above exposed .txt files as well as the electronic energy from the energy.txt file saving them as variables. Having saved the system frequencies as variables the program search in the created strings the "–" character, therefore counting and printing the amount of negative frequencies present in the system. Once the exact amount of negative vibration frequencies has been computed the script prepares the strings as numpy module arrays, a kinder format for its mathematical treatment using python, and cuts the negative frequencies as they do not represent vibrational frequencies and hence having them contributing to the entropy would cause a bias. Once all the frequencies have been prepared, the script asks the user for the initial temperature and the final temperature in K which the program will take to perform the calculation as well as the temperature step used for the computing.

Lastly, the script computes all the Gibbs free energy for each specified temperature thanks to the frequencies and the temperature scale created and writes the results as a two column .txt file named tempgibbs.txt, were the first one represents the temperature at which the Gibbs free energy is calculated for the system and the second one represents the Gibbs free energy for the temperature at its left.

The resulting data allows us to calculate the Gibbs free energy difference between both HS and LS state by subtracting G(LS) to G(HS) (as specified in eq.14) for each temperature in the scale and therefore interpolating the SCO temperature as the temperature which satisfies that $\Delta G = 0$.

In the present work Gibbs free energy has been computed each 10K for a scale between 10K and 1000K. Plotting the Gibbs free energy variation along the specified temperature scale leads to the scatter chart below (figure 1).

The rest of the scatter charts for systems present in the current work are in appendix 2.

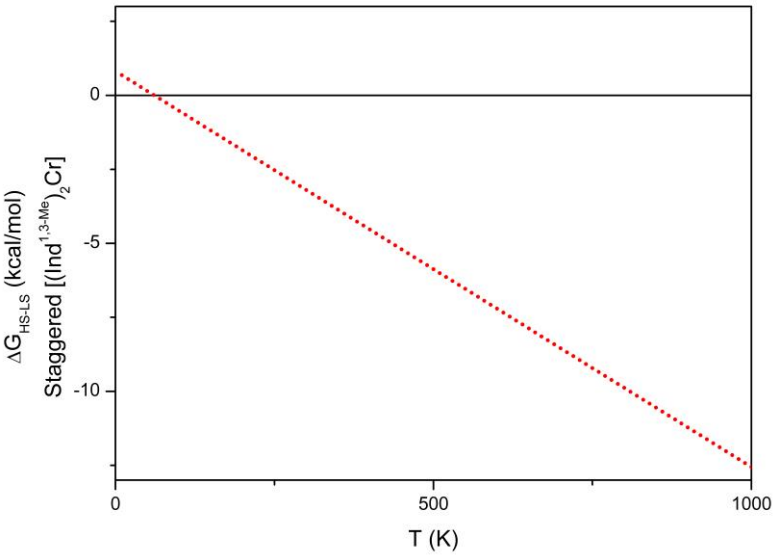

Figure 1. Change in gibbs free energy between HS and LS states (kcal/mol) scatter plotted in front of temperature (K) for [(Ind1,3-Me)2Cr].

7. RESULTS AND DISCUSSION

Along this section SCO properties of the proposed [(Ind^R)$_2$Cr] complexes will be discussed, as well as their structural data.

7.1 DFT BENCHMARK

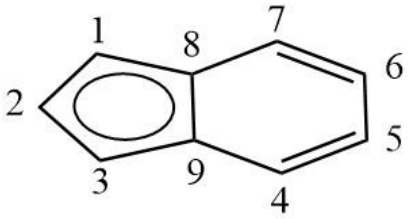

Figure 2. Counting used for indenyl ligand

7.1.1 Benchmarking system election

As only some of the studied complexes have been reported experimentally, the spectrum of the ones which can be chosen as candidates for the calibration is reduced to only a few. The ones with both crystallographic and magnetic measurements, which allow them to become calibration candidates are [(Ind$^{1,2,3\text{-Me}}$)$_2$Cr], [(Ind$^{4,7\text{-Me}}$)$_2$Cr]. and [(Ind$^{2,4,7\text{-Me}}$)$_2$Cr] as polymethylated complexes[9] and [(Ind$^{1\text{-Me}}$)$_2$Cr] and [(Ind$^{2\text{-Me}}$)$_2$Cr] as the monomethylated[10].

Having considered all the reported data for these compounds the chosen one has been [(Ind$^{1,2,3\text{-Me}}$)$_2$Cr]. Owing to its clear shift from the low to the high spin form, which allows an accurate determination of $T_{1/2}$ and solid evidence of the predominant presence of the staggered form over the eclipsed one, [(Ind$^{1,2,3\text{-Me}}$)$_2$Cr] becomes the best candidate for the calibration of the functionals.

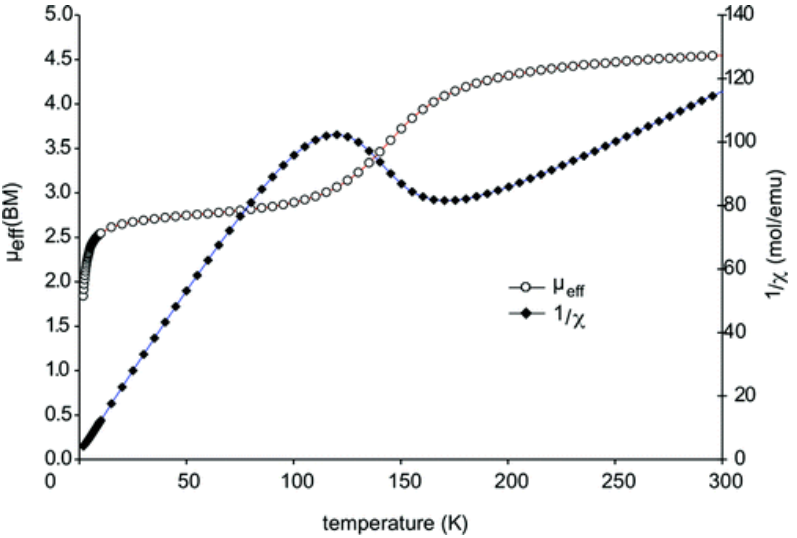

Figure 3. SQUID measurement for $(Ind^{1,2,3\text{-}Me})_2Cr$. Extracted from M. Brett Meredith et al. *Organometallics* **2008**, 27(21), 5464-5473

In Figure 3, we can observe how both values for low and high spin states are consistent with the spin-only values for these (being $2.83\mu_B$ the expected value for a low spin chromium (II) complex owing to its two unpaired electrons, calculated from equation 13, and $4.90\mu_B$ the one expected by a high spin state with four unpaired electrons, value obtained from equation 13 too).

Spin crossover temperature can be obtained from both the μ_{eff} and the $1/\chi$ scattering as they are both, related magnitudes. To obtain the SCO temperature from them, we must know the exact temperature at which μ_{eff} is an inflection point.

7.1.2 Functional benchmarking

In order to resolve which functional captures the best, variations occurred in the electronic structure of the elected system, optimization calculations were performed with eight different functionals, trying to get the wider spectrum of them to obtain an overview of their performance.

Functional	E_{HS} (a.u.)	E_{LS} (a.u.)	E_{HS-LS} (kcal/mol)
OLYP [a]	-1974.87867	-1974.86793	-6.74
OPBE [a]	-1974.85844	-1974.84908	-5.87
M06L [a]	-1974.94937	-1974.94360	-3.62
BLYP [a]	-1974.64273	-1974.64192	-0.51
*B3LYP** [b]	-1966.04639	-1966.03817	-5.16
B3LYP [b]	-1975.09674	-1975.08162	-9.49
TPSSTPSS [a]	-1975.30021	-1975.30380	2.25
TPSSh [b]	-1975.18472	-1975.18062	-2.57

Table 1. Electronic energies and energy differences computed from the optimization calculation of (Ind3Me-1,2,3)2Cr. [a] for pure functionals, [b] for hybrid ones. [c]B3LYP* reduces Hartree-Fock energy contribution from 20% (which is the default in B3LYP) to 15%.

Knowing that spin transition temperature is 150K for (Ind3Me-1,2,3)2Cr low spin state must be the one which is predominant at lower temperatures, and therefore its energy must be lower than the high spin state one (we must remember that calculations were performed in gas phase at 0K). With these statement in mind a valid functional, which correctly captures electronic structure variations happened during the spin transition, must validate a positive energy difference between high spin state and low spin state.

Therefore, in this first approach to the benchmarking of functionals just one valid exchange correlation functional was find, TPSSTPSS, which uses TPSS functional[11] in the depiction of both the correlation and exchange part of the problem. Vibrational frequencies of the system in equilibrium were computed in order to obtain the expected SCO transition temperature from the system with the TPSSTPSS functional.

Expected SCO temperature is 479K. As this temperature is way higher than the experimentally reported (150K) further tools must be used to improve the procedure.

To get a better approximation an empirical correction was benchmarked too, with both TPSSTPSS (for its promising results) and TPSSh (as it is a functional which has been reported to predict with accuracy the enthalpy changes linked to SCO processes[5]) to get a wider overview. Elected empirical correction was GD3BJ, which is in base the D3 version of Grimme's dispersion with the addition of Becke's and John damping function. Empirical dispersion correction focuses

on the performance of minor dispersion forces present in the system to improve the accuracy of DFT calculations.

Results are the following:

Functional	E_{HS} (a.u.)	E_{LS} (a.u.)	E_{HS-LS} (kcal/mol)
TPSSTPSS + GD3BJ	-1975.39626	-1975.40545	5.77
TPSSh + GD3BJ	-1975.27554	-1975.27719	1.03

Table 2. Electronic energies and energy differences between high and low spin states for the elected functionals corrected with GD3BJ empirical dispersion.

As we can see, energy differences computed from both systems are higher once the empirical dispersion correction comes into play. This trend has been reported for further authors as a common feature for empirical dispersion corrections[12]. Specially interesting is how the correction allows TPSSh to be a valid functional for calculations of the energy of the system by increasing its energy difference from -2.57 kcal/mol (a negative difference, which therefore depicts a high-spin only compound which cannot perform spin crossover transition) to 1.03 kcal/mol (a very low energy difference between both states, which should allow SCO fenomena to happen as it is a barrier which can be exceeded by thermal energy). Due to this reduction in the energy difference between both states the SCO temperature is reduced to 113K (150K as observed experimentally), a value in higher consistency with reported experimental data.

Regarding to structural data, Cr-C distances have been reported experimentally[9] and therefore its comparation with the theoretical obtained ones can be taken as another part of the validation method.

		$d(Cr\text{-}C9)_{theoretical}$		$d(Cr\text{-}C)_{theoretical}$ - $d(Cr\text{-}C)_{exp}$	
	$d(Cr\text{-}C)_{exp}$[9]	TPSSh+GD3BJ	TPSSTPSS+GD3BJ	TPSSh+GD3BJ	TPSSTPSS+GD3BJ
d(Cr-C1)	2.209	2.241	2.232	0.032	0.023
d(Cr-C2)	2.219	2.248	2.239	0.029	0.02
d(Cr-C3)	2.201	2.239	2.232	0.038	0.031
d(Cr-C8)	2.282	2.352	2.338	0.07	0.056
d(Cr-C9)	2.283	2.35	2.337	0.067	0.054

Table 3. Interatomic distances comparison between experimentally and theoretically obtained for [(Ind1,2,3-Me)2Cr]

As we can see in table 3, TPSSTPSS+GD3BJ performs a bit better computing bond distances for the present system than TPSSh+GD3BJ. Even though, difference between both functionals is almost non-existent as TPSSh+GD3BJ overestimates Cr-C bond lengths between an 1.3% and a 3% while TPSSTPSS+GD3BJ does the same between a 0.9% and a 2.4% respect the experimentally reported. Therefore, both correlation exchange functionals perform almost at an equal level computing bond distances, when they apply GD3BJ empirical dispersion correction.

The spin-crossover temperature obtained from the TPSSTPSS, GD3BJ corrected calculations is 508K, being even higher than the one obtained without the correction, and as a result data turns down TPSSTPSS to be a valid functional for the depiction of the electronic structure for studied systems.

Considering everything exposed above, the functional which captures the best the electronic structure effects happening in the SCO transition of [$(Ind^{1,2,3\text{-}Me})_2Cr$] is the TPSSh correlation exchange functional together with the GD3BJ empirical dispersion correction.

Therefore, from now on, calculations on the following systems will be performed with them.

7.1.3 Basis set benchmarking

Accuracy of the results based on computational DFT methods are backed up mainly in the correlation exchange functional used as they describe how electrons must be treated, and bonding of atoms as a result, but elected basis set is an important decision as the degree of accuracy of the depiction is decided by it. A bigger basis (referring to a higher amount of base functions used for the calculation) allows a more itemized depiction of the system, but at the cost of a higher computational price.

In order to decide the basis set used in the present work a complete optimization of staggered [$(Ind^{1,2,3\text{-}Me})_2Cr$] system was performed for low and high spin state, in order to elucidate, where the saturation of the basis set occurs (saturation is a phenomena which happens when adding new basis functions don't allows an increase in performance as new functions added are not necessary).

Basis benchmarked were, Def2TZV (with 444 basis functions), Def2QZV (with 614 basis functions), Def2TZVP (with 945 basis functions), Def2TZVPP (with 1172 basis functions) and Def2QZVP (with 2232 basis functions). Number of base functions depends on the basis set chosen, as well as the number and nature of atoms in the system.

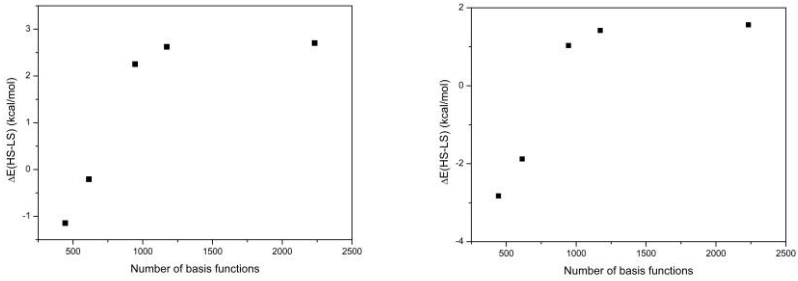

Figure 4. Saturation of the basis sets for the [$(Ind^{1,2,3\text{-}Me})_2Cr$] complex. For both graphs the used basis sets are, in increasing number of base functions, Def2TZV, Def2QZV, Def2TZVP, Def2TZVPP and Def2QZVP. At the left the energy difference is plotted in front of the number of base functions for correlation exchange TPSSTPSS functional. At the right the same is done for TPSSh correlation exchange functional with GD3BJ correction.

Increasing the amount of base functions for performed calculations increased the amount of time required for the calculations to achieve conversion, as a more accurate depiction of the system was being done. In this case Def2QZV, having 614 basis functions, takes double the time to converge than Def2TZV, with 444 basis functions, using the experimentally reported structure as an initial point. For Def2TZVP, with 945 basis functions, convergence takes almost three times more time than for Def2QZV and reaches almost the 3.5 times of time when the Def2TZVPP is the one compared to Def2QZV. Last, but not least Def2QZVP, being the bigger of all benchmarked basis sets, takes three times more time to converge than the next one in the ladder (Def2TZVPP), almost four times from Def2TZVP (which is the more promising one) despite having a bit more than the double of base functions than them.

	Energy difference between HS and LS states (kcal/mol)	
Number of base functions	**TPSSTPSS**	**TPSSh-GD3BJ**
444	-1.14	-2.82
614	-0.21	-1.88
945	2.25	1.03
1172	2.62	1.42
2232	2.70	1.56

Table 4. A table containing the energy differences between HS and LS states.

As we can see in table 4 basis set saturation occurs for bigger basis sets than Def2TZVP being this one the one which offers the most accuracy within the lesser time. Owing to that fact, the one which will be used along the present work will be Def2TZVP.

7.2 IN SILICO DESIGN OF NEW SYSTEMS

Experimentally reported data seems to suggest that the increasing number of methyl groups is related to a higher spin crossover temperature due to the donation of electronic density to ligands.

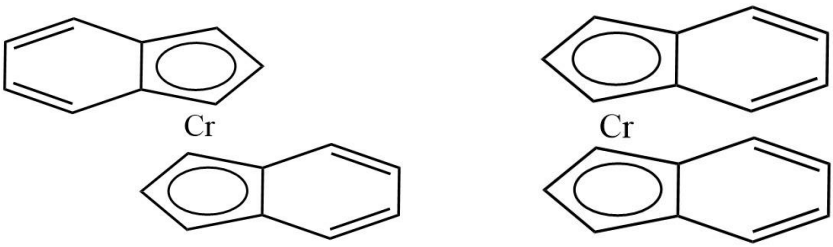

Figure 5. Staggered conformation of ligands (at left) and eclipsed conformation (at right).

In a first attempt to elucidate, optimizations of all the studied systems where carried on in a staggered conformation, as well as frequency calculations of the optimized geometries. Staggered conformation was chosen above eclipsed one to be the firstly studied as most of the experimentally reported systems show priority for this conformation.

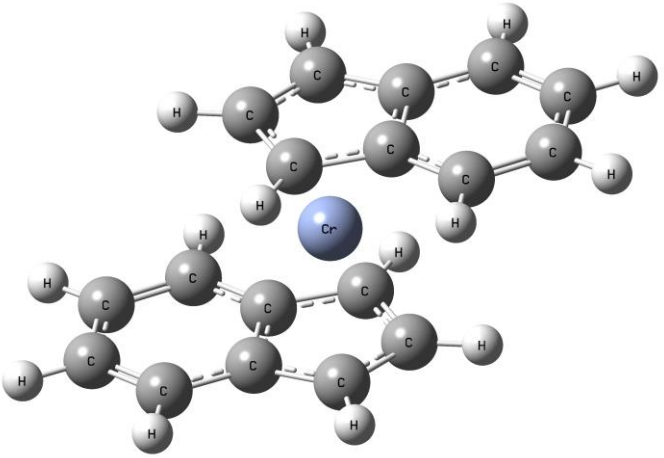

Figure 6. $[(Ind)_2Cr]$ in its staggered conformation and high spin state.

Due to the presence of methyl groups, which can freely rotate, some of the systems presented methodological problems which hindered their convergence. In an attempt to surpass these limitations the convergence factor for density matrix elements was reduced to 10^{-6}, the CalcFC method was used (which specifies that the force constants are calculated at first point) and the CalcAll method was applied to in a last attempt to get to the converged system (CalcAll forces Gaussian to compute force constants at each single point, allowing a better directed optimization).

7.2.1 SCO temperature discussion

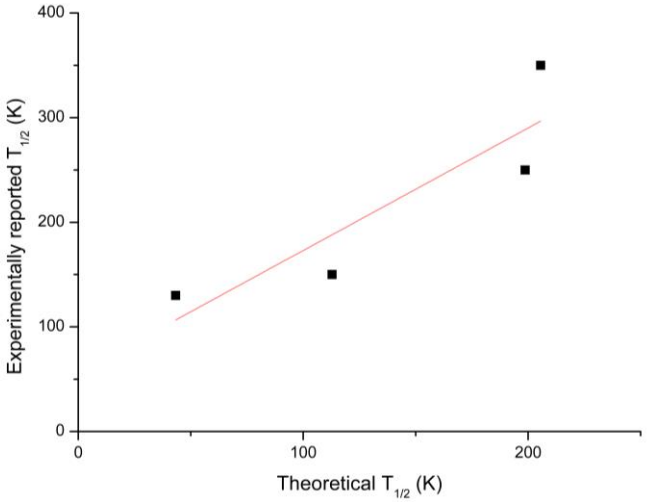

Figure 7. Experimentally reported $T_{1/2}$ vs theoretically obtained $T_{1/2}$.

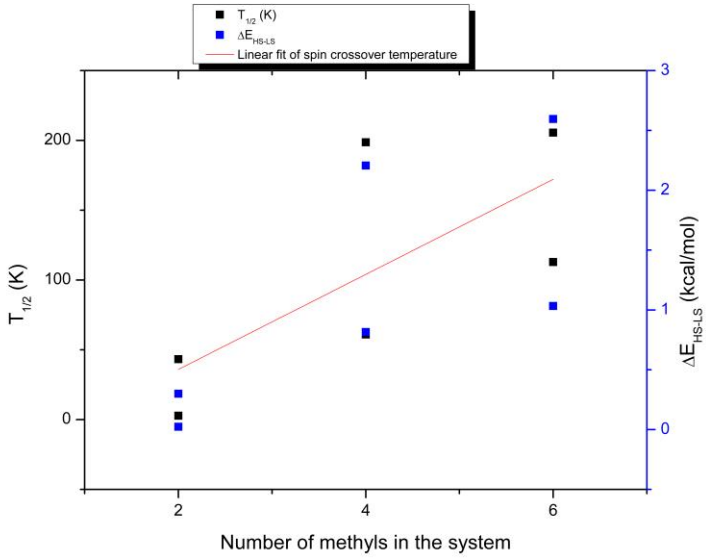

Figure 8. Spin crossover temperature is plotted in front of the number of total methyl groups in the system for all the staggered systems with SCO properties. In the secondary Y axis, the energy difference between high-spin and low-spin state is specified.

System	Number of methyl groups in the system	Theoretical $T_{1/2}$ (K) – Staggered	Experimentally reported $T_{1/2}$ (K)	ΔE_{HS-LS} (kcal/mol)
[(Ind)$_2$Cr]	0	-13	-	-0.15
[(Ind$^{2\text{-}Me}$)$_2$Cr]	2	3	High-spin[10]	0.02
[(Ind$^{1\text{-}Me}$)$_2$Cr]	2	43	130[10]	0.30
[(Ind$^{1,3\text{-}Me}$)$_2$Cr]	4	61	-	0.82
[(Ind$^{1,2,3\text{-}Me}$)$_2$Cr]	6	113	150[9]	1.03
[(Ind$^{4,7\text{-}Me}$)$_2$Cr]	4	199	250[9]	2.21
[(Ind$^{2,4,7\text{-}Me}$)$_2$Cr]	6	206	>350[9]	2.60

Table 5. This table contains the theoretical $T_{1/2}$ for each staggered system (data plotted in figure 8), as well as the electronic energy difference between both states and the experimentally reported data for each system.

Firstly, and regarding table 5, a negative temperature has no sense outside the theory. This just means that the [(Ind)$_2$Cr] system would exhibit HS only behaviour in practice and therefore it would not possess a SCO temperature, as it would not present SCO phenomena. Another remarkable fact regarding [(Ind)$_2$Cr] is, that it has been reported to be stable only in a dimeric form as [(Ind)$_4$Cr$_2$], where two indenyls act as η^5 ligands and two as μ-η^3.[13,14]

Experimentally reported data of [(Ind$^{4,7\text{-}Me}$)$_2$Cr] belongs to the eclipsed conformation and [(Ind$^{2,4,7\text{-}Me}$)$_2$Cr] experimentally reported data belongs to a unit cell containing both the eclipsed and the staggered conformation[9].

[(Ind$^{1,3\text{-}Me}$)$_2$Cr] has no experimental evidence in any of its possible forms, even so, it is a halfway form between entirely five member ring methylated compound, [(Ind$^{1,2,3\text{-}Me}$)$_2$Cr], and five member ring monomethylated compounds, like [(Ind$^{1\text{-}Me}$)$_2$Cr] and [(Ind$^{2\text{-}Me}$)$_2$Cr] which are part of the present work too.

When the theoretical spin-crossover temperature is scatter plotted in front of the experimentally reported temperature (figure 7), one observes how the data obtained from the

multiple calculations for the staggered conformation is consistent with the experimentally reported one. If the theoretically obtained SCO temperature is plotted against the number of methyl groups in the system, with an increasing SCO temperature with the increase of the number of methyl groups in the system, we can determine that the addition of methyl groups to the system stabilizes the low-spin state. These contribute donating electron density to the aromatic system and hence activating it. This increase of the electronic density leads to an increase of the temperature in which both HS and LS states remain in equilibrium with equal quantities of systems in both states, also known as spin-crossover temperature (SCO temperature to shorten it).

Data from Figure 8 and Table 5 seems to suggest that methyl groups attached to the carbons forming the six member ring portion of the ligand have a higher effect on SCO temperature increasing than the ones attached to the five members ring part for present studied systems. Due to this difference in their effect over the SCO temperature change, figure 8 seems to represent two different trend lines.

This is supported by the fact that, for compounds with equal number of methyl groups, the ones with more methyl groups in the six member ring present higher SCO temperatures.

To put it in perspective results must be compared, starting with [(Ind$^{1,3\text{-Me}}$)$_2$Cr] and [(Ind$^{4,7\text{-Me}}$)$_2$Cr] which, despite having the same number of methyl groups, present a huge difference in their SCO temperature, being the one belonging to [(Ind$^{4,7\text{-Me}}$)$_2$Cr] almost 140K higher than the one from [(Ind$^{1,3\text{-Me}}$)$_2$Cr] (nearly 200K in front of 60K). The only difference between both compounds is the location of the methyl groups in the indenyl ligand, which for [(Ind$^{4,7\text{-Me}}$)$_2$Cr] are bonded to the six-member ring part of the ligand and for [(Ind$^{1,3\text{-Me}}$)$_2$Cr] they are bonded to the five member ring.

Another case supporting this hypothesis is the [(Ind$^{1,2,3\text{-Me}}$)$_2$Cr] and [(Ind$^{2,4,7\text{-Me}}$)$_2$Cr] pair, in which, as the pair above, two methyl groups are transferred from the 1,3 positions to the 4,7 ones (being the two first in the five member ring part of the compound and the two last in the six member portion). This permutation has an effect on SCO temperature of more than 90K increasing it from 113K, SCO temperature belonging to [(Ind$^{1,2,3\text{-Me}}$)$_2$Cr], to 205K, SCO temperature belonging to [(Ind$^{2,4,7\text{-Me}}$)$_2$Cr].

Finally, is worth mentioning how when energy difference between both states is plotted on top of the SCO temperatures (as has been done in figure 8) the correlation between the two magnitudes is huge denoting how the entropy variation is similar for all the systems.

7.2.2 Structural discussion: C-C ligand bonds

It is clear then, that the methylation of the indenyl ligands leads to an increase of the electronic density in the ligand rings and, hence, an increase in the SCO temperature along the staggered studied systems.

In this section we will overview how this is reflected in the position of atoms as well as in the length of the bonds.

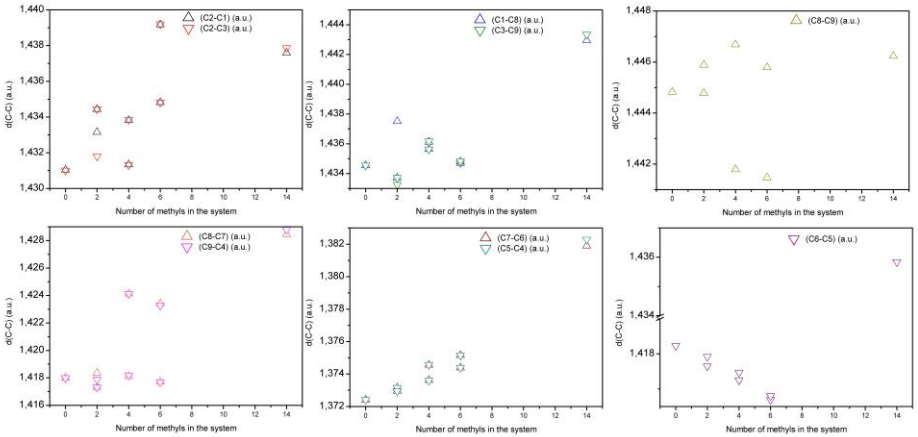

Figure 9. C-C bond lengths are plotted in order to identify their present trends in front of the number of methyl groups of the system for the low-spin state. (Exact data in appendix 3).

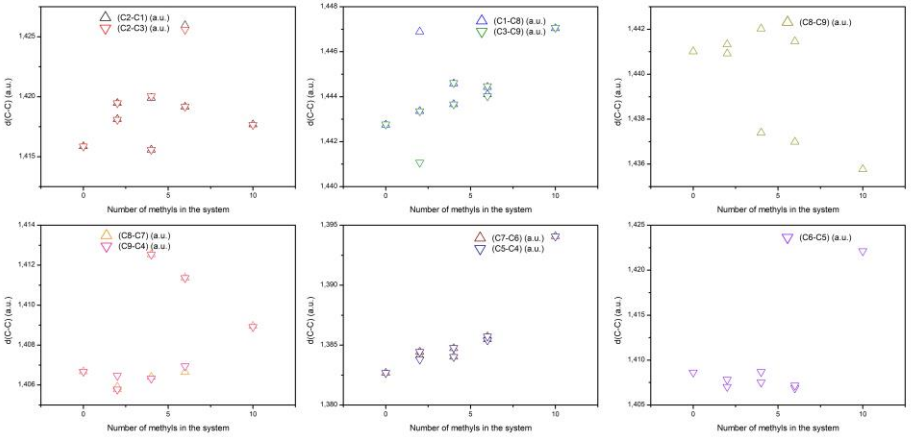

Figure 10. C-C bonds lengths in front of the number of methyl groups attached to the system for the high-spin state. (Exact data in appendix 3)

With a thorough study of the data of figure 9 and figure 10 it is clear that progressive methylation of the indenyl ligand leads to a wide diversity of change trends in their bond lengths.

For C1-C2 and C2-C3 bonds (both symmetric respect to the plane perpendicular to both ligands and therefore equivalent with almost equal behaviour and trends if the symmetry is not broken) in the low-spin case, we can see how the average bond length follows an increasing trend with each added methyl, with an average increase in the bond length higher for each methyl added in the five-member ring portion of the system (carbons C1, C2 and C3).

In the high-spin case the trend is not so clear, as even if there is an increase in the bond length following the same trend as in the low-spin case, the system with the most methyl groups, [(Indenyl$^{2,4,5,6,7\text{-Me}}$)$_2$Cr], is a discordant system with a way lower C1-C2 and C2-C3 bond length than most of the systems and lower than the expected if it followed the tendency.

Even though, this overall increasing trend, reflects how the addition of methyl group to the indenyl ligands, leads to the redistribution of electronic density from both C1-C2 and C2-C3 bonds to another ones, making their lose part of their aromatic bond character as in favour of a single bond character.

A similar trend is followed by C1-C8 and C3-C9 bonds for the high-spin case, gradually losing part of their electronic density with each methyl added to the ligand and, therefore becoming larger weaker bonds. For the low-spin state case, no clear trends are identified due to the absence of any kind of clear statistical pattern.

Following with the increasing bond length trend, C7-C6 and C5-C4 bonds show, for either low or high-spin cases, an increasing length pattern linked to the delocalization of their electronic density to other bonds with each added methyl.

C6-C5 bond seems to be the only bond in the system which unequivocally becomes shorter with the addition of methyl groups in both states. This means that the already said bond increases its double bond character as it increases its electronic density and decreases its length, except for the systems with more methyl groups attached in each state which seem to increase all their C-C bond lengths independently of the overall trend.

Having identified the bonds with clear trends two groups of them remain.

The first lasting bond is the one between C8 and C9, an especially interesting bond as it is the only one in the whole system which is part of both five- and six-member ring parts of the

systems. For the specified bond, the addition of methyl groups to carbons C1, C2 and C3 (the methylable ones forming the five membered ring) leads to a starting increase of the bond length which a slow decrease of it after reaching its maximum length in [(Indenyl$^{1,3\text{-Me}}$)$_2$Cr]. Even though, the addition of methyl groups to carbons forming the six membered ring causes an overwhelming decrease in comparison with the addition of methyl groups to any other portion of the system.

The remaining bond pair is the one formed by C8-C7 and C9-C4 which follows the complementary behaviour with an overall stability of the bond length with the addition of methyl groups to the five membered ring part, but an starting increase and subsequent shortening of the bond length for the addition of methyl groups to the six membered ring portion of the ligand.

With all the arguments exposed above, we could firmly assure that electronic density is being distributed with the addition of methyl groups from C1-C2, C2-C3, C7-C6 and C5-C4 bonds to C6-C5, lengthening the first and shortening the last.

7.2.3 Structural discussion: Cr-C bond

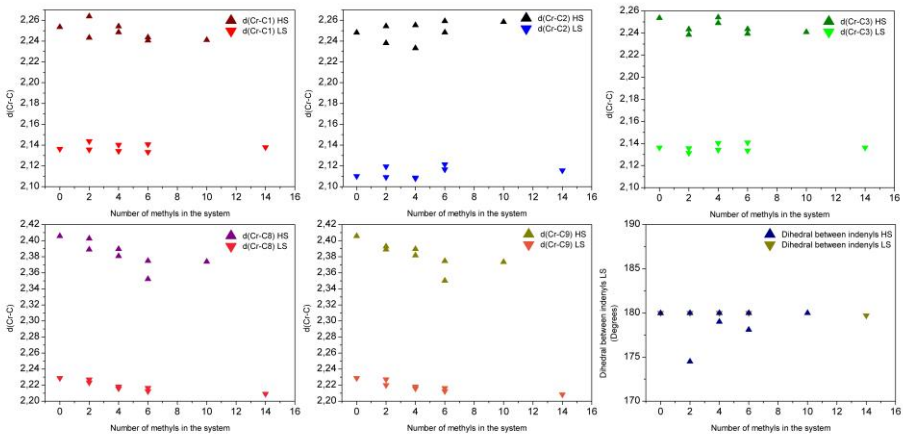

Figure 11. An analysis of the variation of the length in C-Cr bonds for the staggered system in both states, as well as the dihedral angle between both indenyl ligands. Exact data at appendix 3

Next step of analysis, which must be done, as it reports relevant data about the structure of the studied systems, is the one regarding the ligand metal bond length. As can be seen in figure 11, systems tend to reduce their metal-ligand Cr-C8 and Cr-C9 bond lengths as more methyl groups are added to the indenyl ligands.

One trend major importance, which can be clearly observed in figure 11, as well as in raw bond length data (present in appendix 3), is the one which follows all the present compounds as they transition from their LS to their HS state, lengthening their bonds unequally (bonds are lengthened as electrons are occupying higher energy orbitals, and therefore, weakening the metal-ligand bond). This difference in the bond length increasing is explained as for the LS state, indenyl ligands are bonded to the metal chromium centre with a higher hapticity than the same system in HS state. Even if for these systems the difference is subtle, we will see later the importance of identifying this behaviour early in the present work.

7.3 ECLIPSED CONFORMATION

Having seen above exposed arguments, one question comes to light as a matter of fact. Structural differences between methyl position isomers, allow huge differences between systems, so will the relative positions of the ligands affect in the same measure the SCO properties?

To elucidate how the isomeric nature of the studied compounds will tune SCO temperature, optimization and frequencies calculations were performed for the studied systems with the same setting as the above ones, but with eclipsed ligand conformation. Eclipsed conformation was chosen over the gauche one for the present work as some of the experimentally reported compounds were proved to show preference for the eclipsed conformation.

7.3.1 SCO temperature discussion

System	Number of methyl groups in the system	Theoretical $T_{1/2}$ (K) – Eclipsed structure	Theoretical $T_{1/2}$ (K) – Staggered	ΔE_{HS-LS} (kcal/mol)
[(Ind)$_2$Cr]	0	206	-13	0.87
[(Ind$^{2\text{-Me}}$)$_2$Cr]	2	-	3	-
[(Ind$^{1\text{-Me}}$)$_2$Cr]	2	418	43	1.00
[(Ind$^{1,3\text{-Me}}$)$_2$Cr]	4	-	61	-
[(Ind$^{1,2,3\text{-Me}}$)$_2$Cr]	6	-	113	-
[(Ind$^{4,7\text{-Me}}$)$_2$Cr]	4	455	199	2.06
[(Ind$^{2,4,7\text{-Me}}$)$_2$Cr]	6	372	206	2.49

Table 6. Theoretical SCO temperature comparison between staggered and eclipsed conformations.

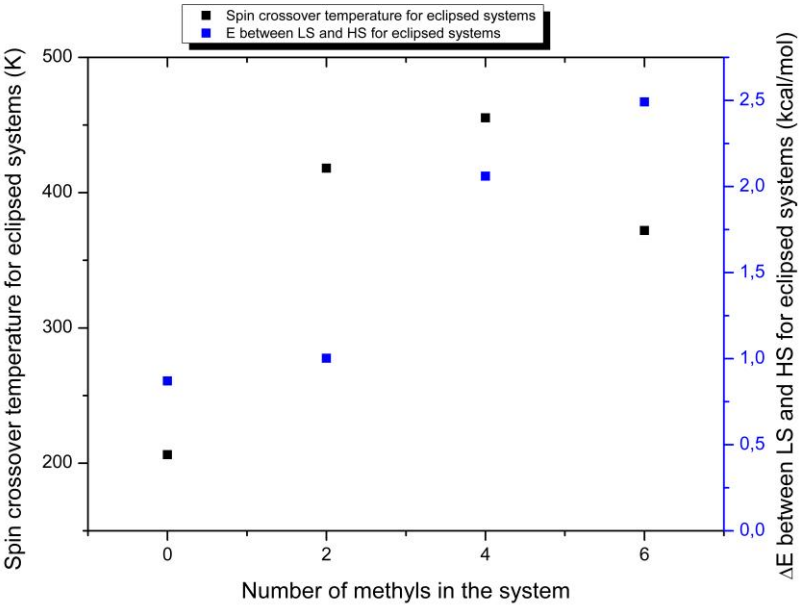

Figure 12. SCO temperature in front of the number of methyl groups in the systems.

All computed temperatures are higher than the ones calculated for its staggered counterpart. This trend leads to compounds which were low-spin only cases to perform as SCO complexes, $[(Ind)_2Cr]$ and $[(Ind^{2\text{-}Me})_2Cr]$ for the matter of this work. An overall weak increasing trend is insinuated even if the correlation is very weak due to the lower than expected SCO temperature in $[(Ind^{2,4,7\text{-}Me})_2Cr]$.

An explanation to this enormous variation in SCO temperature with a change which, at least at first sight, could seem minimal can be found in figure 13.

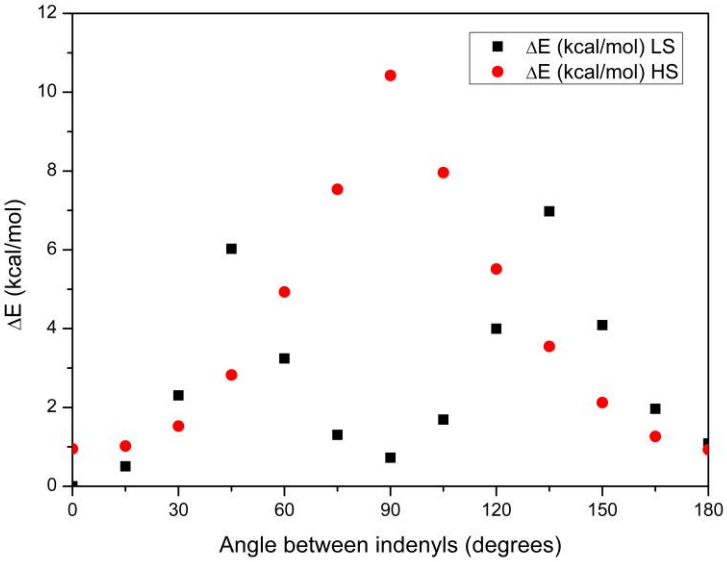

Figure 13. Rigid scan of the PES for the rotation of one indenyl ligand respect to another for [(Ind)$_2$Cr] system.

As figure 13 evince, changes in the relative orientation of the ligands, one respect another, cause subtle changes in the system's overall energy. The explanation of why those little changes have a huge impact in SCO temperature remains in entropy. As seen in equations 14, 16 and 17, entropy plays a main role determining the SCO temperature as it will tip the scales in favour of HS or LS state, determining which one will be the predominant in each temperature, and therefore, determining the temperature at which transition from one to another will take part.

For studied systems electronic entropy changes from LS state to HS state which perform a crucial paper in SCO phenomena, happen to be the minimum among SCO complexes as chromium (II) is a d^4 metal which transitions from a S=1 with two unpaired electrons LS state to a S=2 with four unpaired electrons HS state. Table 7 shows some entropic changes computed from equation 16 with the $\mathbf{\Delta}H = \mathbf{\Delta}E_{el}$ approximation for the studied systems which achieved good enough optimizations to report only positive frequencies (and therefore to achieve a truly stationary point).

System	Conformation	ΔS_{HS-LS} (cal/mol*K)
$[(Ind^{2\text{-}Me})_2Cr]$	Staggered	7.78
$[(Ind^{1\text{-}Me})_2Cr]$	Eclipsed	2.39
$[(Ind^{4,7\text{-}Me})_2Cr]$	Eclipsed	4.53
$[(Ind^{2,4,7\text{-}Me})_2Cr]$	Eclipsed	6.70

Table 7. Entropy variation from HS to LS state for selected systems.

Hence, the fewer than average entropy variation for studied systems results in huge changes in SCO temperature with small changes in energy difference between both states allowing, for better or worse enormous, changes in it with little modifications in the complex's structure.

7.3.2 Structural discussion: C-C ligand bonds

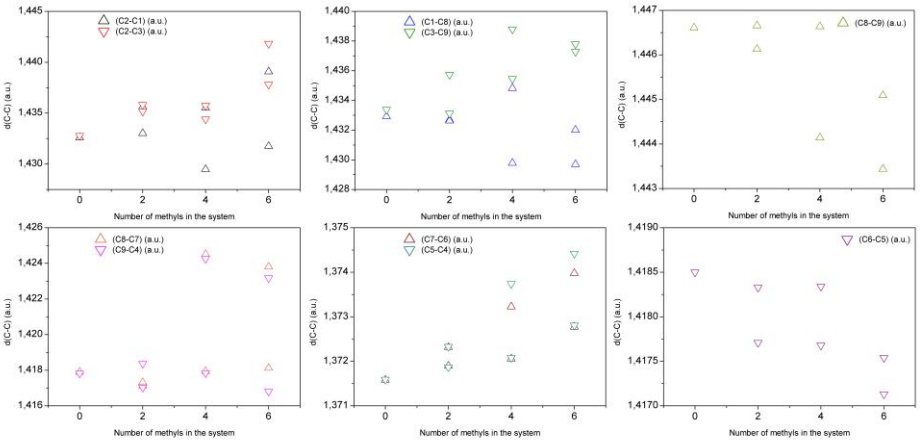

Figure 14. C-C bond lengths in indenyl ligand for the LS system

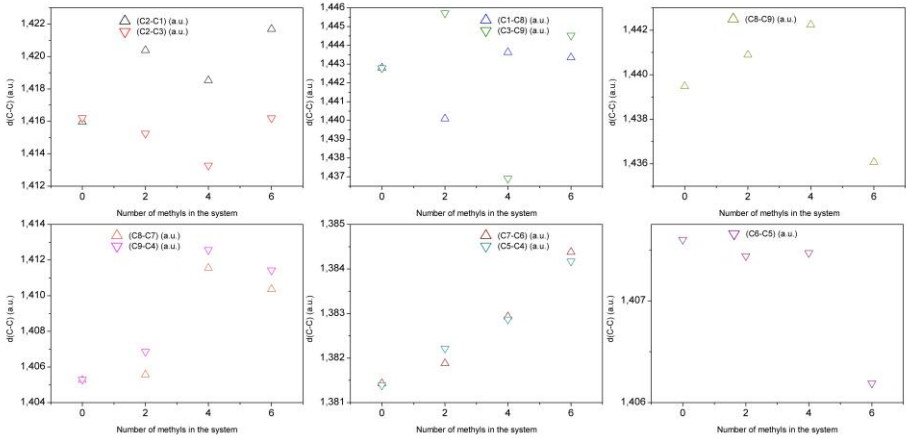

Figure 15. C-C bond lengths in indenyl ligand for the HS system

Regarding the influence exerted by methyl groups attached to the indenyl ligands of systems, similar trends to staggered conformation are extracted from the C-C bond lengths of eclipsed conformation with C1-C2 and C2-C3 bonds increasing its length with each new methyl attached to the ligand for the LS spin system. C8-C9 bond length becomes smaller in LS state with each methyl added to the six-member ring portion of the ring, a trend which is lost for the HS state (in which we have too few systems to extract any conclusion).

Again, in C8-C7 and C9-C4 bonds become larger with the addition of methyls to the six-member ring portion of the ligand for the LS state, not having enough information to elucidate its tendency for the HS one.

C7-C6 and C5-C4 bonds become unequivocally larger with each added methyl for either states and, once more, C6-C5 bond seems to gather the electronic density which other bonds have lost by shortening its own distance.

7.3.3 Structural discussion: Cr-C bond

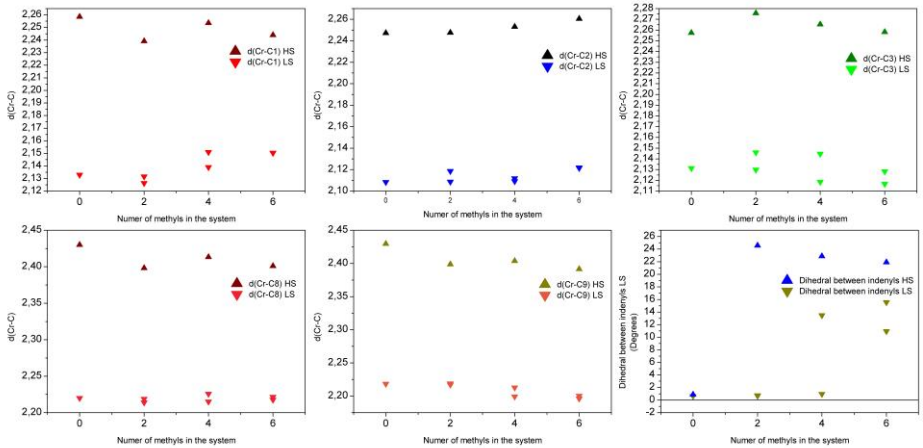

Figure 16. Analysis of the Cr-C bond length and the dihedral angle between both indenyl ligands. Distances in a.u. (data in appendix 3)

In figure 16 can be appreciated that the addition of methyl groups attached to the ligand does not affect the Cr-C2 bond length in LS state, but increases it in the HS one.

Regarding LS state, special interest arises from Cr-C1 bond as it becomes larger with each methyl added in detriment of its symmetric pair the Cr-C3 bond which becomes shorter as more methyl groups are attached to the ligand. Thus, the ligand approaches one of its sides to the chromium atom while it is separated from it on the other side.

The small change of hapticity seen before in staggered conformation becomes clearer in this conformation as the difference in the bond lengths becomes larger between LS and HS states.

Main differences between both eclipsed and staggered states happens to be in the dihedral angle between both states. Eclipsed conformations create a higher repulsion between both, now facing, indenyl ligands, species with π-electronic densities. To stabilize these systems ligands now try to adopt conformations where the electronic density present in the rings of both ligands becomes further one from each other, distorting the angles formed between them. This distortion becomes higher with each methyl added to the ligand, for the LS state, as they provide the ligand rings with more electronic density. The addition of methyl groups to the six-ring portion of the ligands creates a bigger distortion in the dihedral between both than the ones attached to the five-member ring part. Regarding the HS state, and due to the lack of more systems, no differences

can be observed between the positioning of the methyl groups. So, no further information can be extracted from it apart from the fact that the addition of the first methyl groups forces ligands to move, creating an enormous distortion in their dihedral which is eased with the addition of new methyl groups to them.

7.4 EFFECT OF SUBSTITUTION OF METHYL GROUPS BY ANOTHER ONES

At this point, and as can be seen in above sections, effects of methyl groups have been studied for both conformations and for diverse systems.

To go one step further in tunability of SCO properties for [(Ind$^{x\text{-}Me}$)$_2$Cr] systems, methyl group was substituted by some other groups with different electron donative power. [(Ind$^{1\text{-}Me}$)$_2$Cr] in eclipsed conformation was the elected system to perform substitutions of methyl groups as it is a system which performed specially well in calculations.

In order to replace methyl groups amino (-NH_2), cyano (-CN), fluorine (-F) and acido (-N_3) groups were chosen, therefore obtaining [(Ind$^{1\text{-}NH2}$)$_2$Cr], [(Ind$^{1\text{-}CN}$)$_2$Cr], [(Ind$^{1\text{-}F}$)$_2$Cr] and [(Ind$^{1\text{-}N3}$)$_2$Cr].

7.4.1 SCO temperature discussion

Hammett parameters	Ligand	System	$T_{1/2}$ (K)	$\Delta E_{HS\text{-}LS}$ (Kcal/mol)
-0.66	*-NH_2*	[(Ind$^{1\text{-}NH2}$)$_2$Cr]	124	0.86
-0.17	*-Me*	[(Ind$^{1\text{-}Me}$)$_2$Cr]	418	0.87
0.06	*-F*	[(Ind$^{1\text{-}F}$)$_2$Cr]	125	0.36
0.08	*-N_3*	[(Ind$^{1\text{-}N3}$)$_2$Cr]	336	1.16
0.66	*-CN*	[(Ind$^{1\text{-}CN}$)$_2$Cr]	505	0.98

Table 8. Substituted ligands and their $T_{1/2}$ and energy difference between both states.

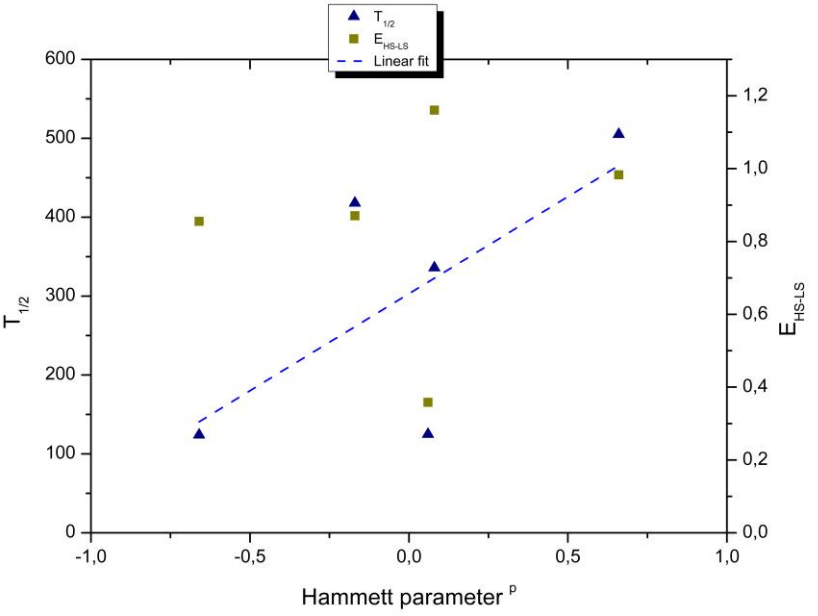

Figure 17. $T_{1/2}$ and $\Delta E_{(HS-LS)}$ are scatter plotted for each system against the para- Hammett parameter of the substitute group

As can be seen from table 8 and figure 17, SCO temperature seems to be related, for studied substituent groups with its para- Hammett parameter (σ^p). Those are related to the reaction speed and equilibrium constant variations suffered by an organic reaction containing a substituted aromatic compound, as a mere contribution of the substituent via the Hammett equation. Hammett parameters have been widely used in organic chemistry as they successfully predict variations in the electronic donating power of substitutes attached to benzene type systems, even if they have been criticised by the theoretical community due to its empirical nature.[15,16]

In the present work they seem to act as a good qualitatively predictive tool to approximate the SCO temperature of a substituted compound, as has been shown with $[(Ind^{1-R})_2Cr]$ systems, with the only remarkable exception of fluorine substituted compound, which is widely separated from the rest of the data. Even though, specially cyano, amino and acido substituted compounds are almost perfectly described by its SCO temperature variation linearly depending from its para-Hammett parameter.

Despite everything, we must remember that, Hammett parameters are not developed in order to describe indenyl systems, and therefore their prediction are not to be taken quantitatively but qualitatively. Group calculated, for past studies, Hammett parameters for other systems, not benzenic, and found out that its scale and order remain like the ones used in benzenic systems.

Taft parameters where considered too for the same job and the same reasons, but Hammett parameters were finally chosen as further information has been found about them.

Apart from Hammett parameters, it has been demonstrated how the modification of the substituent present in indenyl ligand tunes the SCO temperature of the whole compound, as it has enough influence over the ligand to noticeably modify its SCO properties, as well as their electronic energy difference between both HS and LS states.

7.4.2 Structural discussion: C-C ligand bonds

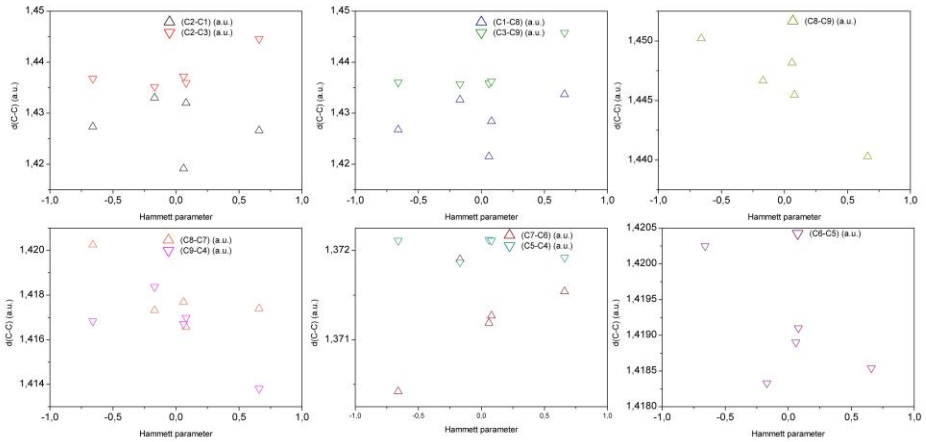

Figure 18. C-C bond lengths for substituted systems in LS state.

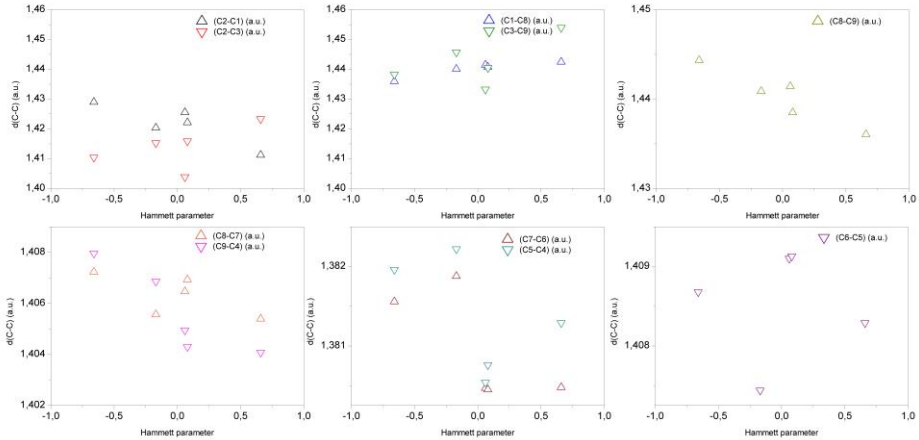

Figure 19. C-C bond lengths for substituted systems in HS state.

An increasing Hammett parameter seems to be correlated to a distribution of electronic density for LS state from C1-C8 and C3-C9 bonds to C6-C5 and C8-C9 bonds (the ones which do not have a symmetric partner). Electronic density redistribution from C1-C8 and C3-C9 pair to C8-C9, can be observed in HS state case too, leading to an increase of bond length of bonds losing electronic density and a lowering of bond length for the ones which are getting more electronic density.

For LS state C8-C7 and C9-C4 pair seems to lose its symmetry as Hammett parameter is separated from 0. This phenomenon can be observed for C2-C1 and C2-C3 pair as well for both states.

In all above cases, we can appreciate the exception of fluorine substituted system, which presents a rather unsymmetrical bond pair for both symmetry losing bond pairs, as well as a different electronic density redistribution pattern. We can therefore conclude, having in mind that for SCO temperature fluorine substituted system was a discordant point too, that Hammett parameters, even if they define with a surprisingly good accuracy trends happened in other systems, are not a good approximation to the electronic donative power of fluorine, and maybe, to halogens as an extent.

7.4.3 Structural discussion: Cr-C bond

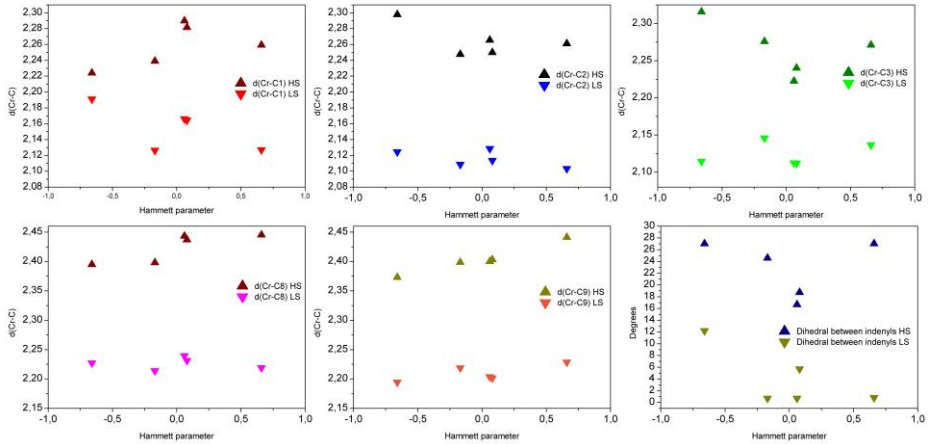

Figure 20. Cr-C bond lengths are scatter plotted in order to identify its trends following the Hammett parameter of indenyl's substituent.

Being C1 the indenyl's carbon which is attached to the substituent and C3 its opposite, we can observe how difference in distance between HS and LS states for the metallic centre and C1 gets higher once Hammett parameter increases and how Cr-C3 distance difference is reduced. For the studied systems this would mean that within SCO phenomena, for low Hammett parameters, Cr-C1 distance remains almost unaltered in comparison with those systems having a high Hammett parameter substituent and Cr-C3 having the opposite behaviour. As a conclusion, low Hammett parameter substituted systems would perform during SCO phenomenon a higher seesaw movement, by hugely increasing its Cr-C3 distance while almost keeping its Cr-C1 distance unaltered and not doing this movement for high Hammett parameters substituted systems, as values for both Cr-C1 and Cr-C3 bond lengths are closer each other, for both states.

Lastly, all of them suffer from the hapticity change exposed in above sections becoming more μ^3 in their HS states and approximately being penta-hapto, μ^5, compounds in their LS states. Not enough data is available to evaluate if the change in Hammett parameters affect in any sense to this hapticity variation. No evidences present that the change in electronic donating power should be affected by electronic donating power of substituents.

7.5 AILFT STUDY ON PRESENT SYSTEMS' ORBITALS

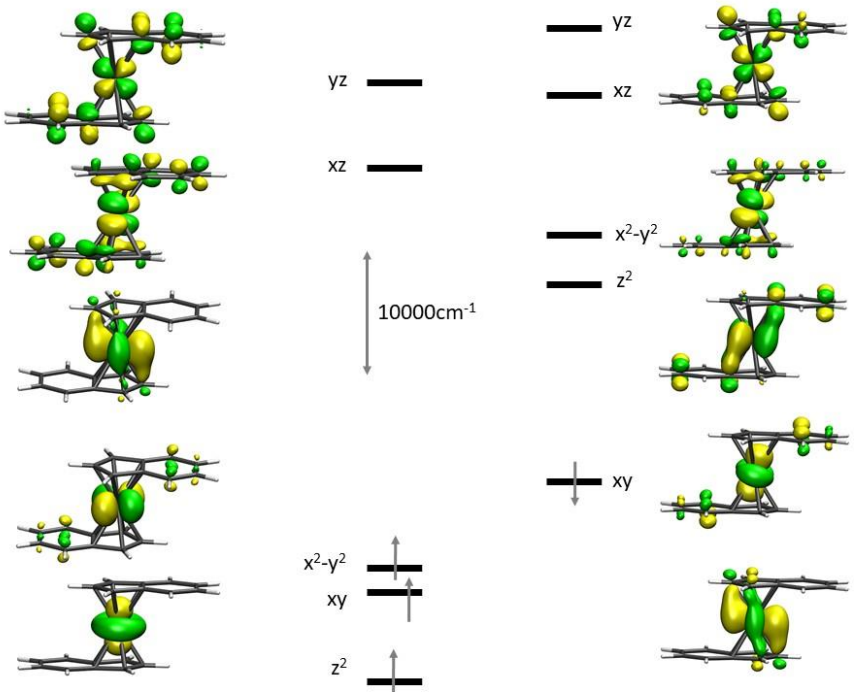

Figure 21. MO diagram for staggered [(Ind)2Cr], from DFT orbitals.

System	Conformation	E(Nonbonding) orbitals (cm^{-1})			E(Antibonding) orbitals (cm^{-1})		10Dq (cm^{-1})
[(Ind$^{1\text{-}Me}$)$_2$Cr]	*Staggered*	0	2570.2	3050.4	18381.8	23745.3	15331.4
[(Ind$^{1,2,3\text{-}Me}$)$_2$Cr]	*Staggered*	0	2239.7	2892.4	18677.8	24333.1	15785.4
[(Ind$^{2,4,7\text{-}Me}$)$_2$Cr]	*Staggered*	0	2452.6	3000.3	18961.6	23600.7	15961.3
[(Ind)$_2$Cr]	*Eclipsed*	0	2876.3	3069.3	20108.9	24412.9	17039.6
[(Ind$^{1\text{-}Me}$)$_2$Cr]	*Eclipsed*	0	2717.3	2954.0	20237.1	24732.7	17283.1
[(Ind$^{4,7\text{-}Me}$)$_2$Cr]	*Eclipsed*	0	2491.4	2867.9	20346.8	23893.6	17478.9
[(Ind$^{1,2,3\text{-}Me}$)$_2$Cr]	*Eclipsed*	0	2411.4	2747.8	20316.0	24994.3	17568.2

Table 9. Orbitals' energy obtained with AILFT.

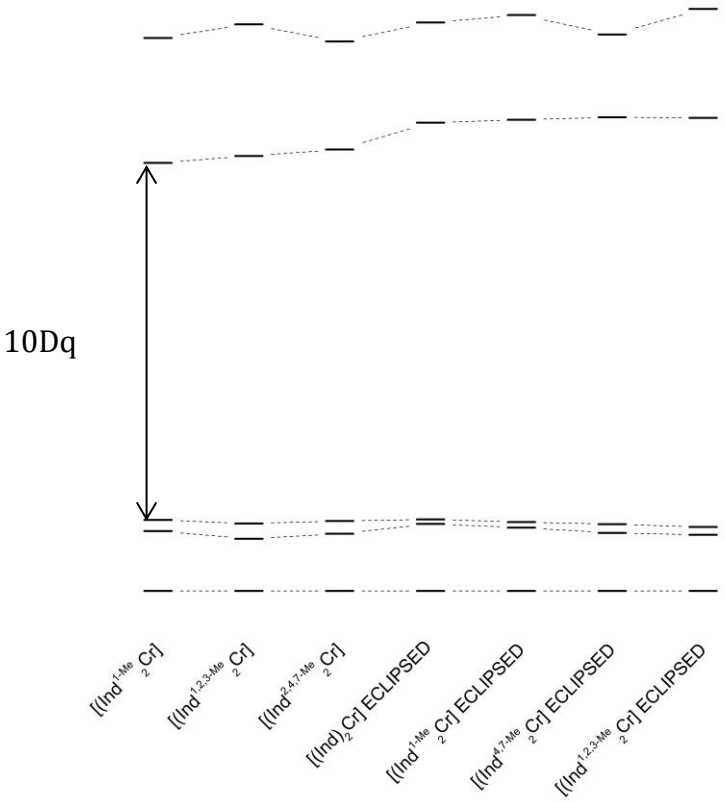

Figure 22. Diagram of orbital energies for AILFT studied systems

AILFT allows us to obtain an accurate depiction of how energy difference between both nonbonding and antibonding orbitals vary with the functionalization of indenyl ligands.

To do so, AILFT normalizes all the orbitals' energies taking the lowest metallic d-orbital in each system as the zero-energy point. This normalization allows us to easily compute 10Dq ligand field parameter as the difference between the HOMO and LUMO orbitals for the LS case, which happen to be the highest energy nonbonding orbital and the lowest energy antibonding orbital.

10Dq parameter is widely used in ligand field theories as it allows to compute and understand rather than complex properties belonging coordination compounds. One of those properties happens to be the total spin of the complex (as explained in section 5.5). In this case 10Dq increases as the number of methyl groups attached to indenyl ligand becomes higher. It increases

for the change between staggered and eclipsed conformations being higher for the second one (as happened with SCO temperature). This effect is produced by an overall increase of the relative orbital energy from antibonding HOMO respect lowest energy orbital. LUMO orbital remains almost equal in energy for every system.

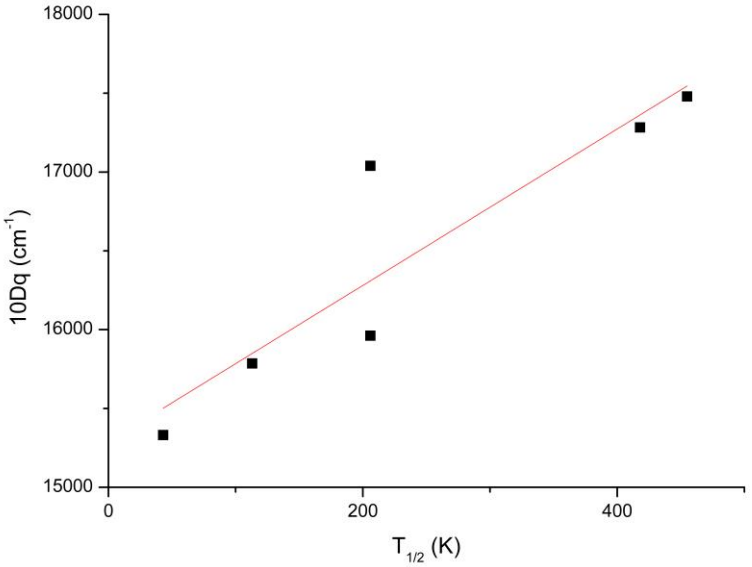

Figure 23. Correlation between $T_{1/2}$ and 10Dq.

Higher importance remains on figure 23, as remarks how 10Dq and $T_{1/2}$ correlate, and therefore, it shows how functionalization of the indenyl ligand, which increases $T_{1/2}$ as has been demonstrated on previous sections, increases the 10Dq parameter, affecting a change done to the ligand to electronic structure of the metallic centre tuning the metal d-orbitals splitting.

We can conclude thanks to it, that small modifications on the indenyl ligand affect how metallic d-orbitals split.

8 CONCLUSIONS

After gathering and processing all the computed data, one can withdraw the following conclusions:

- The present work validates TPSSh correlation exchange functional when used together with GD3BJ empirical dispersion correction as a suitable methodology for the study of SCO properties, and electronic structure to an extent, from indenyl chromium (II) systems.
- Def2TVZP happens to be a big enough basis set to capture the electronic structure effects studied in the present work.
- Theoretical results produced in the present work, with above explained methodology, faithfully reproduce experimental data and increase the actual knowledge of SCO properties of indenyl chromium (II) complexes.
- Position of methyl groups in indenyl ligand hugely affect the SCO behaviour of the whole complex, being the effect produced by the ones attached to the six-membered ring (C4 and C7 where studied) bigger than the ones attached to the five-membered ring. Even in the five-ring attached subset, methyl group bonded to C1 and C3 seem to induce a higher increase in SCO temperature, than the ones attached to C2.
- The substitution of methyl groups, by another ones, with different electron donating properties allows some fine tuning of SCO properties.
- Has been proved how systems studied in the present work possess low electronic entropies. This fact produces the range of energy differences between both HS and LS states which allows SCO phenomenon to happen, to be shorter than for other SCO systems. Another consequence of the low entropy, is that due to eq.14, even little changes in energy difference between states lead to high changes in SCO temperature, as for example changes in system's conformation from staggered to eclipsed.

9 REFERENCES AND NOTES

1. Olguín, J. Unusual metal centres/coordination spheres in spin crossover compounds. *Coord. Chem. Rev.* **407**, (2020).
2. Hohenberg, P. & Kohn, W. Inhomogeneous Electron Gas. *Phys. Rev.* **136**, 864–871 (1964).
3. Sham, W. K. L. J. Self-Consistent Equations Including Exchange and Correlation Effects. *Phys. Rev.* **140**, 1133–1138 (1965).
4. Schleder, G. R., Padilha, A. C. M., Acosta, C. M., Costa, M. & Fazzio, A. From DFT to machine learning: recent approaches to materials science–a review. *J. Phys. Mater.* **2**, 032001 (2019).
5. Cirera, J. & Paesani, F. Theoretical prediction of spin-crossover temperatures in ligand-driven light-induced spin change systems. *Inorg. Chem.* **51**, 8194–8201 (2012).
6. Cirera, J. & Ruiz, E. Computational Modeling of Transition Temperatures in Spin-Crossover Systems. *Comments Inorg. Chem.* **39**, 216–241 (2019).
7. Gütlich, P. & Jung, J. Thermal and optical switching of iron(II) compounds. *J. Mol. Struct.* **347**, 21–38 (1995).
8. Kumar, S., Eng, J., Atanasov, M. & Neese, F. Covalency and chemical bonding in transition metal complexes : An ab initio based ligand field perspective. *Coord. Chem. Rev.* **344**, 2–25 (2017).
9. Meredith, M. B. *et al.* Tunable spin-crossover behavior in polymethylated bis(indenyl)chromium(II) complexes: The significance of benzo-ring substitution. *Organometallics* **27**, 5464–5473 (2008).
10. Meredith, M. B. *et al.* High-spin and spin-crossover behavior in monomethylated bis(indenyl)chromium(II) complexes. *Organometallics* **25**, 4945–4952 (2006).
11. Tao, J. & Perdew, J. P. Climbing the Density Functional Ladder : Nonempirical Meta – Generalized Gradient Approximation Designed for Molecules and Solids. **91**, 3–6 (2003).
12. Cirera, J., Via-nadal, M. & Ruiz, E. Benchmarking Density Functional Methods for Calculation of State Energies of First Row Spin-Crossover Molecules. *Inorg. Chem.* **57**, 14097–14105 (2018).
13. Heinemann, O., Jolly, P. W., Krüger, C. & Verhovnik, G. P. J. Bis(indenyl)chromium is a dimer. *Organometallics* **15**, 5462–5463 (1996).
14. Zouchoune, B., Zendaoui, S. M. & Saillard, J. Y. Why is bis-indenylchromium a dimer? A DFT investigation. *J. Organomet. Chem.* **858**, 47–52 (2018).
15. Hammett, L. P. & Hammett, B. L. P. The Effect of Structure upon the Reactions of Organic Compounds . Benzene Derivatives Reactivity. **125**, 96–103 (1936).
16. Hansch, C., Leo, A. & Taft, R. W. A Survey of Hammett Substituent Constants and Resonance and Field Parameters log Kh. 165–195 (1991) doi:10.1021/cr00002a004.

10 ACRONYMS

SCO = spin-crossover

$T_{1/2}$ = spin-crossover temperature

DFT = density functional theory

LDA = local density approximation

GGA = general gradient approximation

mGGA = meta-general gradient approximation

HS = high-spin state

LS = low-spin state

PES = potential energy surface

NEVPT2 = second order n-electron valency perturbation theory

CASSCF = complete active space self-consistent field

[$(Ind)_2Cr$] = bis(indenyl)chromium (II)

[$(Ind^{1\text{-}Me})_2Cr$] = bis(1-methylindenyl)chromium (II)

[$(Ind^{2\text{-}Me})_2Cr$] = bis(2-methylindenyl)chromium (II)

[$(Ind^{1,3\text{-}Me})_2Cr$] = bis(1,3-dimethylindenyl)chromium (II)

[$(Ind^{4,7\text{-}Me})_2Cr$] = bis(4,7-methylindenyl)chromium (II)

[$(Ind^{1,2,3\text{-}Me})_2Cr$] = bis(1,2,3-trimethylindenyl)chromium (II)

[$(Ind^{2,4,7\text{-}Me})_2Cr$] = bis(2,4,7-trimethylindenyl)chromium (II)

[$(Ind^{2,4,5,6,7\text{-}Me})_2Cr$] = bis(2,4,5,6,7-pentamethylindenyl)chromium (II)

[$(Ind^{1,2,3,4,5,6,7\text{-}Me})_2Cr$] = bis(1,2,3,4,5,6,7-heptamethylindenyl)chromium (II)

APPENDICES

APPENDIX 1: PYTHON3 SCRIPT USED TO COMPUTE SCO TEMPERATURES OF THE SYSTEMS

```
#Script to calculate gibbs energy from the harmonic frequencies of a system
#Numpy module is loaded in order to calculate with arrays
import numpy

#Frequencies archives are opened and read:
freqs1=open("freqs1.txt","r")
freqs2=open("freqs2.txt","r")
freqs3=open("freqs3.txt","r")
e=open("energy.txt","r")

freqs1=(freqs1.read())
freqs2=(freqs2.read())
freqs3=(freqs3.read())
e=(e.read())
e=float(e)

#Arrays' length is calculed
l1=int((len(freqs1)))
l2=int((len(freqs2)))
l3=int((len(freqs3)))

#The total number of negative freqs is calculed for the three inputs
m=0
for i in range (l1):
    if freqs1[i]=="-":
        m=m+1
```

```
    else:
        None
for i in range (l2):
    if freqs2[i]=="-":
        m=m+1
    else:
        None
for i in range (l3):
    if freqs3[i]=="-":
        m=m+1
    else:
        None
print("Number of total negative frequencies:",m)

#The input arrays are converted to numeric arrays

if m==1:
    freqs1=freqs1[9:-1]
elif m==2:
    freqs1=freqs1[9:-1]
    freqs2=freqs2[9:-1]
elif m==3:
    freqs1=freqs1[9:-1]
    freqs2=freqs2[9:-1]
    freqs3=freqs3[9:-1]
else:
    None
freqs1=freqs1.split()
freqs2=freqs2.split()
freqs3=freqs3.split()

freqs=(freqs1+freqs2+freqs3)
```

```
freqs=numpy.array(freqs)
freqs=freqs.astype(numpy.float)

#Temperatures are required
t1=int(input("Initial temperature: "))
t2=int(input("Final temperature: "))
step=int(input("Size of the step: "))
lt=(t2-t1)/(step)
p=lt-int(lt)
if p!=0:
   print("!BEWARE WITH THE STEP SIZE")
else:
   None
temp_array=numpy.linspace(t1,t2,lt+1)

#Gibbs is computed from the freqs resulting string

kb=1.38064852E-23
hv=freqs*6.62607004E-34
au2kcalmol=627.509541
J2kcalmol=1.44E20
tempgibbs=open("tempgibbs.txt","w")
for i in range(len(temp_array)):
   kbt=temp_array[i]*kb
   exponential=numpy.exp((hv/kbt)*(-1))
   ones=numpy.ones(len(exponential))
   entropy=kbt*J2kcalmol*numpy.sum(numpy.log(ones-exponential))
   gibbs=e*au2kcalmol+entropy
   temp=str(temp_array[i])
   gibbs=str(gibbs)
   tempgibbs.write(temp+" "+gibbs+"\n")
```

APPENDIX 2: ΔG VS T DELS SISTEMES ESTUDIATS

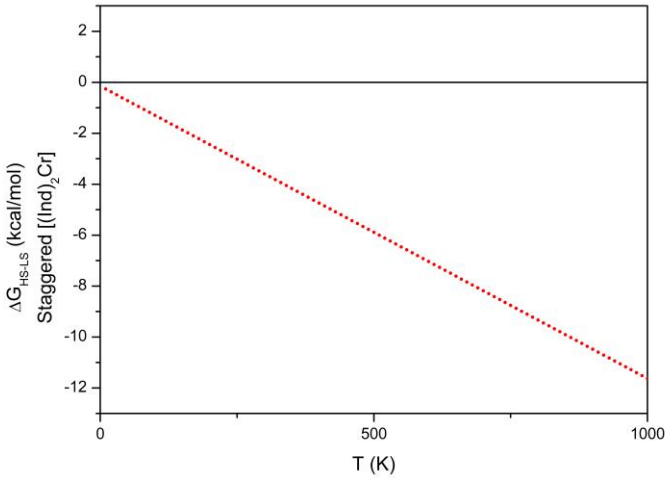

Figure 24. Gibbs energy difference between HS and LS states vs temperature for vs temperature for [(Ind)$_2$Cr] in staggered conformation.

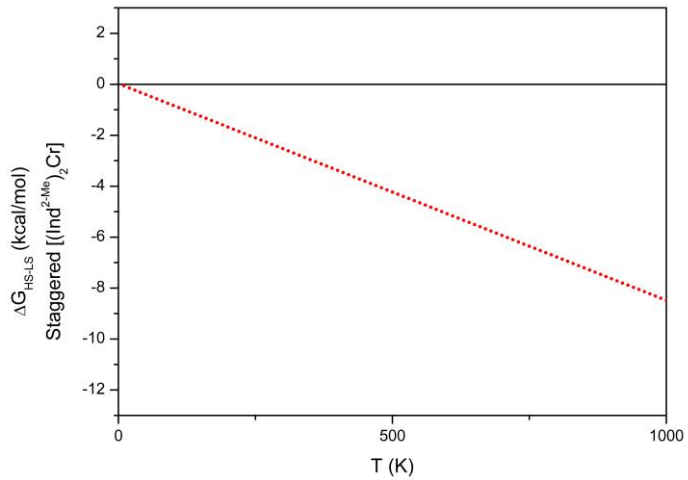

Figure 25. Gibbs energy difference between HS and LS states vs temperature for vs temperature for [(Ind^{2-Me})$_2$Cr] in staggered conformation.

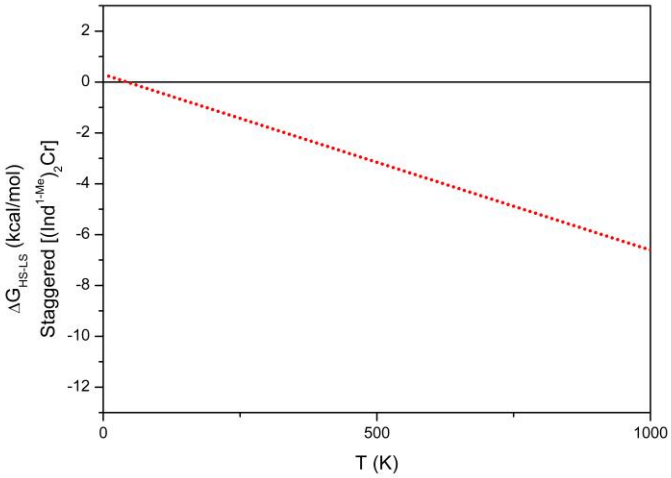

Figure 26. Gibbs energy difference between HS and LS states vs temperature for $[(Ind^{1\text{-}Me})_2Cr]$ in staggered conformation.

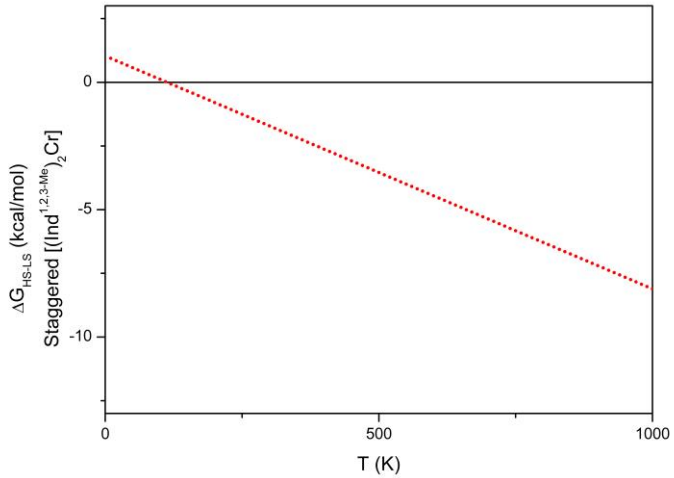

Figure 27. Gibbs energy difference between HS and LS states vs temperature for $[(Ind^{1,2,3\text{-}Me})_2Cr]$ in staggered conformation.

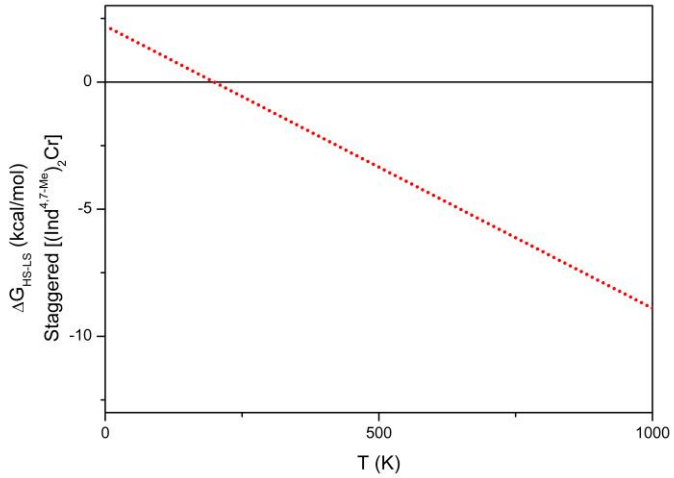

Figure 28. Gibbs energy difference between HS and LS states vs temperature for [(Ind$^{4,7\text{-Me}}$)$_2$Cr] in staggered conformation.

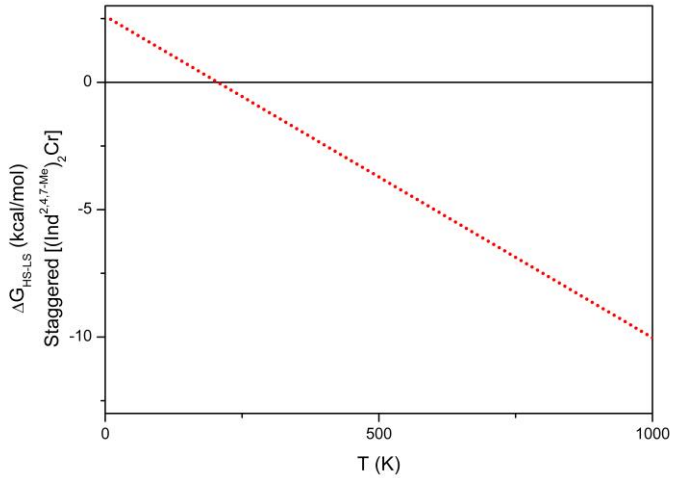

Figure 29. Gibbs energy difference between HS and LS states vs temperature for [(Ind$^{2,4,7\text{-Me}}$)$_2$Cr] in staggered conformation.

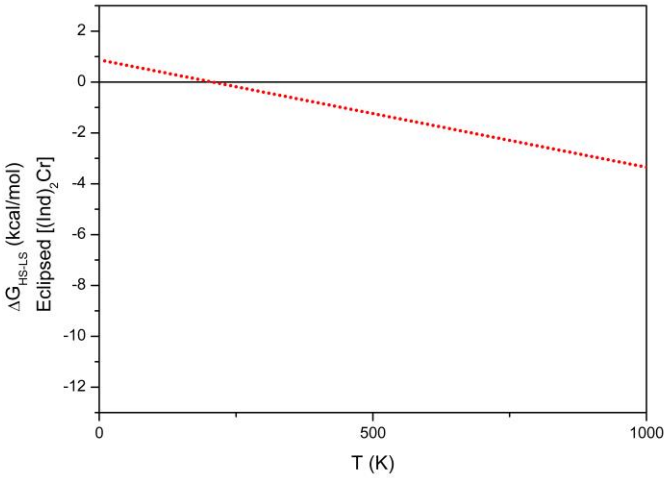

Figure 30. Gibbs energy difference between HS and LS states vs temperature for $[(Ind)_2Cr]$ in staggered conformation.

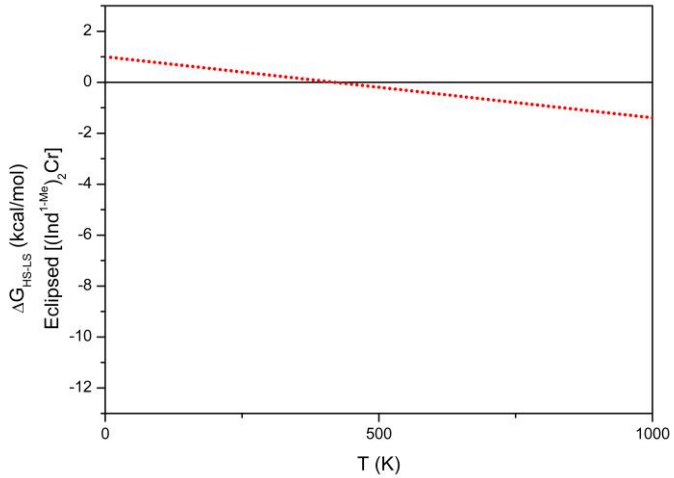

Figure 31. Gibbs energy difference between HS and LS states vs temperature for $[(Ind^{1\text{-}Me})_2Cr]$ in eclipsed conformation.

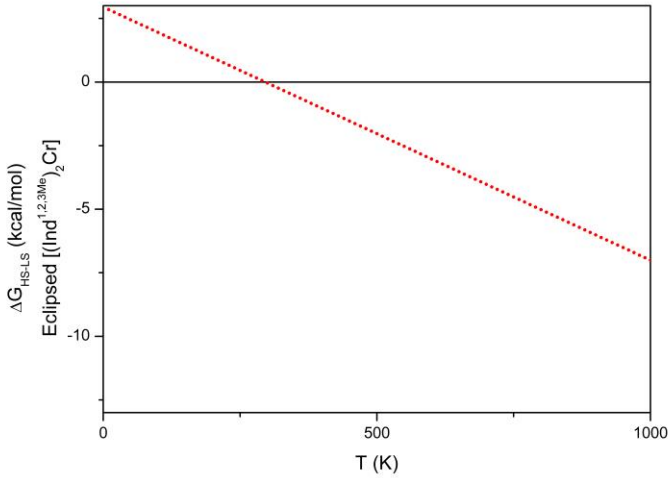

Figure 32. Gibbs energy difference between HS and LS states vs temperature for [(Ind$^{1,2,3\text{-Me}}$)$_2$Cr] in eclipsed conformation.

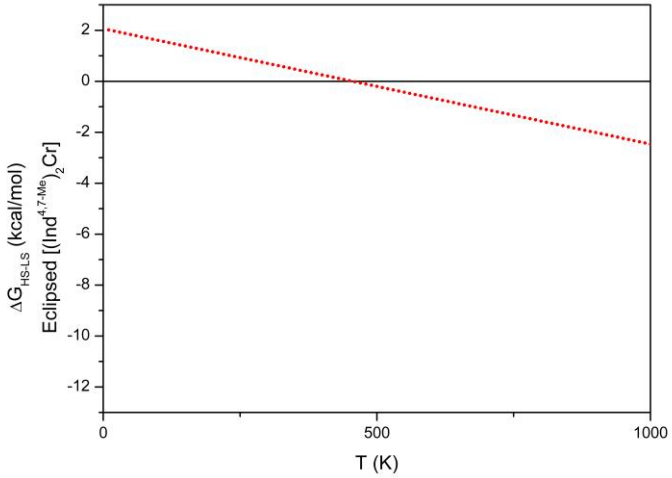

Figure 33. Gibbs energy difference between HS and LS states vs temperature for [(Ind$^{4,7\text{-Me}}$)$_2$Cr] in eclipsed conformation.

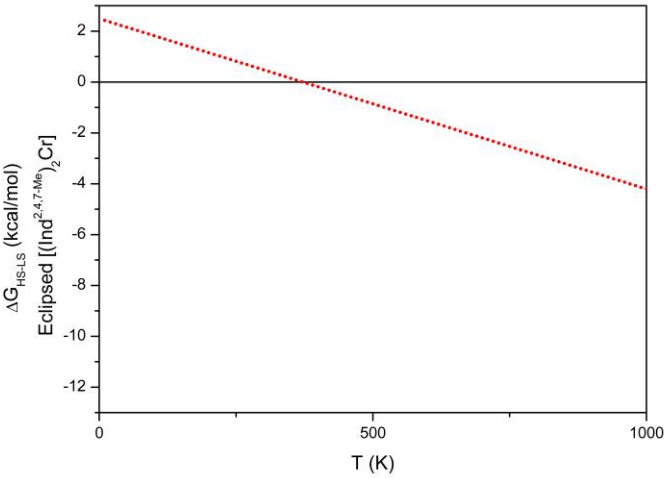

Figure 34. Gibbs energy difference between HS and LS states vs temperature for $[(Ind^{2,4,7\text{-}Me})_2Cr]$ in eclipsed conformation.

APPENDIX 3: STRUCTURAL DATA

System	d(C2-C1)	d(C2-C3)	d(C1-C8)	d(C3-C9)	d(C8-C9)
[(Ind)$_2$Cr]	1.43104	1.43101	1.43455	1.43455	1.44483
[(Ind$^{2\text{-Me}}$)$_2$Cr]	1.43444	1.43444	1.43371	1.43372	1.44478
[(Ind$^{1\text{-Me}}$)$_2$Cr]	1.43316	1.4318	1.43751	1.43326	1.44589
[(Ind$^{1,3\text{-Me}}$)$_2$Cr]	1.43382	1.43385	1.43613	1.43618	1.44669
[(Ind$^{1,2,3\text{-Me}}$)$_2$Cr]	1.43917	1.43920	1.43471	1.43472	1.44579
[(Ind$^{4,7\text{-Me}}$)$_2$Cr]	1.43134	1.43132	1.43564	1.43563	1.44179
[(Ind$^{2,4,7\text{-Me}}$)$_2$Cr]	1.43482	1.43482	1.43480	1.43484	1.44147
[(Ind$^{1,2,3,4,5,6,7\text{-Me}}$)$_2$Cr]	1.43759	1.43786	1.44295	1.44335	1.44624

System	d(C8-C7)	d(C9-C4)	d(C7-C6)	d(C5-C4)	d(C6-C5)
[(Ind)$_2$Cr]	1.41800	1.41799	1.37241	1.37242	1.41823
[(Ind$^{2\text{-Me}}$)$_2$Cr]	1.41731	1.41731	1.37315	1.37315	1.41765
[(Ind$^{1\text{-Me}}$)$_2$Cr]	1.41837	1.41787	1.37296	1.37294	1.41792
[(Ind$^{1,3\text{-Me}}$)$_2$Cr]	1.41811	1.41819	1.37362	1.37360	1.41747
[(Ind$^{1,2,3\text{-Me}}$)$_2$Cr]	1.41771	1.41769	1.37439	1.37439	1.41669
[(Ind$^{4,7\text{-Me}}$)$_2$Cr]	1.42413	1.42412	1.37456	1.37457	1.41725
[(Ind$^{2,4,7\text{-Me}}$)$_2$Cr]	1.42341	1.42328	1.37517	1.37516	1.41680
[(Ind$^{1,2,3,4,5,6,7\text{-Me}}$)$_2$Cr]	1.42846	1.42880	1.38191	1.38229	1.43584

Table 10. C-C bond lengths for the LS state of staggered systems. All distances are in a.u.

System	d(C2-C1)	d(C2-C3)	d(C1-C8)	d(C3-C9)	d(C8-C9)
[(Ind)$_2$Cr]	1.41586	1.41585	1.44275	1.44277	1.44101
[(Ind$^{2\text{-}Me}$)$_2$Cr]	1.41946	1.41946	1.44336	1.44336	1.44092
[(Ind$^{1\text{-}Me}$)$_2$Cr]	1.41813	1.41808	1.44689	1.44107	1.44133
[(Ind$^{1,3\text{-}Me}$)$_2$Cr]	1.41989	1.42004	1.44458	1.44461	1.44203
[(Ind$^{1,2,3\text{-}Me}$)$_2$Cr]	1.42595	1.42559	1.4441	1.44402	1.44146
[(Ind$^{4,7\text{-}Me}$)$_2$Cr]	1.41558	1.41558	1.44366	1.44366	1.4374
[(Ind$^{2,4,7\text{-}Me}$)$_2$Cr]	1.41916	1.41917	1.44443	1.44447	1.43699
[(Ind$^{2,4,5,6,7\text{-}Me}$)$_2$Cr]	1.41768	1.41766	1.44704	1.44707	1.43577

System	d(C8-C7)	d(C9-C4)	d(C7-C6)	d(C5-C4)	d(C6-C5)
[(Ind)$_2$Cr]	1.40668	1.40667	1.38267	1.38268	1.40862
[(Ind$^{2\text{-}Me}$)$_2$Cr]	1.40578	1.40578	1.38444	1.38444	1.40703
[(Ind$^{1\text{-}Me}$)$_2$Cr]	1.40591	1.40646	1.38412	1.38380	1.40782
[(Ind$^{1,3\text{-}Me}$)$_2$Cr]	1.40640	1.40632	1.38473	1.38478	1.40751
[(Ind$^{1,2,3\text{-}Me}$)$_2$Cr]	1.40665	1.40695	1.38548	1.38540	1.40687
[(Ind$^{4,7\text{-}Me}$)$_2$Cr]	1.41254	1.41253	1.38402	1.38403	1.40868
[(Ind$^{2,4,7\text{-}Me}$)$_2$Cr]	1.41137	1.41136	1.38572	1.38573	1.40717
[(Ind$^{2,4,5,6,7\text{-}Me}$)$_2$Cr]	1.40896	1.40891	1.39408	1.39407	1.42212

Table 11. C-C bond lengths for the HS state of staggered systems. All distances are in a.u.

System	d(Cr-C1)	d(Cr-C2)	d(Cr-C3)	d(Cr-C8)	d(Cr-C9)	Dihedral angle between indenyls
[(Ind)$_2$Cr]	2.13625	2.11018	2.13629	2.22890	2.22886	180.0
[(Ind$^{2\text{-}Me}$)$_2$Cr]	2.13574	2.11937	2.13572	2.22705	2.22707	180.0
[(Ind$^{1\text{-}Me}$)$_2$Cr]	2.14375	2.10918	2.13134	2.22324	2.21998	180.0
[(Ind$^{1,3\text{-}Me}$)$_2$Cr]	2.14020	2.10868	2.14034	2.21590	2.21593	180.0
[(Ind$^{1,2,3\text{-}Me}$)$_2$Cr]	2.14078	2.12149	2.14078	2.21243	2.21247	180.0
[(Ind$^{4,7\text{-}Me}$)$_2$Cr]	2.13424	2.10807	2.13424	2.21819	2.21823	180.0
[(Ind$^{2,4,7\text{-}Me}$)$_2$Cr]	2.13328	2.11655	2.13361	2.21646	2.21639	180.0
[(Ind$^{1,2,3,4,5,6,7\text{-}Me}$)$_2$Cr]	2.13786	2.11556	2.13623	2.20911	2.20833	179.7

Table 12. Cr-C bond lengths for the LS state of staggered systems. All distances are in a.u. Dihedral is measured in degrees.

System	d(Cr-C1)	d(Cr-C2)	d(Cr-C3)	d(Cr-C8)	d(Cr-C9)	Dihedral angle between indenyls
[(Ind)$_2$Cr]	2.25363	2.24828	2.25359	2.40576	2.40571	179.98
[(Ind$^{2\text{-}Me}$)$_2$Cr]	2.24337	2.25443	2.24339	2.38895	2.38897	180.0
[(Ind$^{1\text{-}Me}$)$_2$Cr]	2.26387	2.23808	2.23840	2.40269	2.39280	174.5
[(Ind$^{1,3\text{-}Me}$)$_2$Cr]	2.24857	2.23316	2.24908	2.38081	2.38167	179.0
[(Ind$^{1,2,3\text{-}Me}$)$_2$Cr]	2.24062	2.24843	2.23928	2.35219	2.35017	178.1
[(Ind$^{4,7\text{-}Me}$)$_2$Cr]	2.25424	2.25535	2.25419	2.38955	2.38950	180.0
[(Ind$^{2,4,7\text{-}Me}$)$_2$Cr]	2.24366	2.25923	2.24350	2.37482	2.37459	180.0
[(Ind$^{2,4,5,6,7\text{-}Me}$)$_2$Cr]	2.24112	2.25843	2.24086	2.37376	2.37333	180.0

Table 13. Cr-C bond lengths for the HS state of staggered systems. All distances are in a.u. Dihedral is measured in degrees.

System	d(C2-C1)	d(C2-C3)	d(C1-C8)	d(C3-C9)	d(C8-C9)
$[(Ind)_2Cr]$	1.43261	1.43278	1.43292	1.43338	1.44661
$[(Ind^{2\text{-}Me})_2Cr]$	1.43563	1.43582	1.43269	1.43313	1.44613
$[(Ind^{1\text{-}Me})_2Cr]$	1.43302	1.43517	1.43264	1.43573	1.44666
$[(Ind^{1,3\text{-}Me})_2Cr]$	1.43552	1.43575	1.43482	1.43545	1.44664
$[(Ind^{1,2,3\text{-}Me})_2Cr]$	1.43909	1.44183	1.43201	1.43728	1.44509
$[(Ind^{4,7\text{-}Me})_2Cr]$	1.42949	1.43441	1.42978	1.4388	1.44414
$[(Ind^{2,4,7\text{-}Me})_2Cr]$	1.43176	1.43781	1.42969	1.43781	1.44344

System	d(C8-C7)	d(C9-C4)	d(C7-C6)	d(C5-C4)	d(C6-C5)
$[(Ind)_2Cr]$	1.41789	1.41782	1.37158	1.37159	1.4185
$[(Ind^{2\text{-}Me})_2Cr]$	1.41711	1.41703	1.37232	1.37233	1.41771
$[(Ind^{1\text{-}Me})_2Cr]$	1.41732	1.41837	1.37190	1.37187	1.41833
$[(Ind^{1,3\text{-}Me})_2Cr]$	1.41794	1.41784	1.37206	1.37208	1.41834
$[(Ind^{1,2,3\text{-}Me})_2Cr]$	1.41813	1.41681	1.37277	1.37281	1.41754
$[(Ind^{4,7\text{-}Me})_2Cr]$	1.42451	1.42426	1.37323	1.37374	1.41768
$[(Ind^{2,4,7\text{-}Me})_2Cr]$	1.42381	1.42318	1.37398	1.37442	1.41713

Table 14. C-C bond lengths for the LS state of eclipsed systems. All distances are in a.u.

System	d(C2-C1)	d(C2-C3)	d(C1-C8)	d(C3-C9)	d(C8-C9)
[(Ind)$_2$Cr]	1.41596	1.41621	1.44281	1.44279	1.43948
[(Ind$^{1\text{-}Me}$)$_2$Cr]	1.42039	1.41525	1.4401	1.44572	1.44089
[(Ind$^{4,7\text{-}Me}$)$_2$Cr]	1.41853	1.41328	1.44364	1.43691	1.44224
[(Ind$^{2,4,7\text{-}Me}$)$_2$Cr]	1.42169	1.4162	1.44335	1.44453	1.43608

System	d(C8-C7)	d(C9-C4)	d(C7-C6)	d(C5-C4)	d(C6-C5)
[(Ind)$_2$Cr]	1.40527	1.40529	1.38143	1.38139	1.4076
[(Ind$^{1\text{-}Me}$)$_2$Cr]	1.40557	1.40686	1.38188	1.38222	1.40744
[(Ind$^{4,7\text{-}Me}$)$_2$Cr]	1.41156	1.41257	1.38293	1.38287	1.40747
[(Ind$^{2,4,7\text{-}Me}$)$_2$Cr]	1.41037	1.41143	1.38438	1.38417	1.40619

Table 15. C-C bond lengths for the HS state of eclipsed systems. All distances are in a.u.

System	d(Cr-C1)	d(Cr-C2)	d(Cr-C3)	d(Cr-C8)	d(Cr-C9)	Dihedral angle between indenyls
[(Ind)$_2$Cr]	2.13295	2.10837	2.13124	2.2199	2.21833	0.7
[(Ind$^{2\text{-}Me}$)$_2$Cr]	2.13161	2.11858	2.12987	2.21879	2.21725	0.7
[(Ind$^{1\text{-}Me}$)$_2$Cr]	2.12627	2.10872	2.14599	2.21385	2.21887	0.7
[(Ind$^{1,3\text{-}Me}$)$_2$Cr]	2.13901	2.10917	2.1448	2.2152	2.21287	1.0
[(Ind$^{1,2,3\text{-}Me}$)$_2$Cr]	2.15038	2.122	2.12836	2.21767	2.20032	11.0
[(Ind$^{4,7\text{-}Me}$)$_2$Cr]	2.15099	2.11185	2.11859	2.22571	2.19918	13.5
[(Ind$^{2,4,7\text{-}Me}$)$_2$Cr]	2.15033	2.12148	2.1166	2.22163	2.1961	15.6

Table 16. Cr-C bond lengths for the LS state of the eclipsed system. All distances are in a.u. Dihedral is measured in degrees.

System	d(Cr-C1)	d(Cr-C2)	d(Cr-C3)	d(Cr-C8)	d(Cr-C9)	Dihedral angle between indenyls
$[(Ind)_2Cr]$	2,25857	2,24724	2,25742	2,43007	2,42947	0,9
$[(Ind^{1\text{-}Me})_2Cr]$	2,23918	2,24756	2,27579	2,39813	2,39871	24,6
$[(Ind^{4,7\text{-}Me})_2Cr]$	2,2536	2,25312	2,26536	2,41343	2,40379	22,9
$[(Ind^{2,4,7\text{-}Me})_2Cr]$	2,24395	2,26053	2,25829	2,40097	2,39157	21,9

Table 17. Cr-C bond lengths for the HS state of the eclipsed system. All distances are in a.u. Dihedral is measured in degrees.